prediction of the changes of the Walsh diagram due to a change of the central atom A.

These qualitative ideas can be used to understand the inversion barrier in AH_3 radicals and their substituted analogues as well as barriers to pyramidalization in AH_3 cations and their substituted analogues.[19]

Acknowledgment. We wish to thank the donors of the Petroleum Research Fund administered by the American Chemical Society, and the Research Corporation for partial support of this research.

References and Notes

(1) J. Lambert, *Top. Stereochem.*, **6**, 19 (1971).
(2) J. D. Swaken and J. A. Ibers, *J. Chem. Phys.*, **36**, 1914 (1962).
(3) J. M. Lehn and B. Munsch, *Chem. Commun.*, 1327 (1969).
(4) A. D. Walsh, *J. Chem. Soc.*, 2260 (1953), and paper thereafter; B. M. Gimarc, *J. Am. Chem. Soc.*, **93**, 593 (1971).
(5) M. J. S. Dewar, "The Molecular Orbital Theory of Organic Chemistry", McGraw-Hill, New York, N.Y., 1969.
(6) H. C. Longuet-Higgins and M. de V. Roberts, *Proc. R. Soc. London, Ser. A*, **224**, 336 (1954); **230**, 110 (1955); R. Hoffmann and W. N. Lipscomb, *J. Chem. Phys.*, **36**, 2179, 3489 (1962); **37**, 2872 (1962); R. Hoffmann, *ibid.*, **40**, 2745 (1964).
(7) Similar reasoning is apparent in a treatment of AX_2 molecules in W. T. Borden, "Modern Molecular Orbital Theory for Organic Chemists", Prentice-Hall, Englewood Cliffs, N.J., 1975, p 136, footnote 1.
(8) J. A. Pople and D. L. Beveridge, "Approximate Molecular Orbital Theory", McGraw-Hill, New York, N.Y., 1970. The d orbitals were suppressed in the calculations of the third-row elements.
(9) L. S. Bartell and R. C. Hirst, *J. Chem. Phys.*, **31**, 449 (1959); E. D. Palik and E. E. Bell, *ibid.*, **26**, 1093 (1951).
(10) J. M. Lehn, A. Veillard, and B. Munsch, *Theor. Chim. Acta*, **9**, 275 (1968).
(11) J. M. Lehn and B. Munsch, *Mol. Phys.*, **23**, 91 (1971).
(12) The interaction between the Ap_z AO and ϕ_1 and the interaction between the As AO and ϕ_1 gives rise to a coupling. This coupling is manifested by a small repulsion between the $(Ap_z + \phi_1)$ MO and the $(As + \phi_1)$ MO initially formed by the union of the A atom and H_3 fragment. For this reason, the lone pair orbital in the pyramidal molecule is higher in energy than the degenerate pair of MO's. Since overlap has been neglected, this repulsion has no net energetic effect. In general, neglect of overlap is justified because two electron-stabilizing effects are more important than four electron-destabilizing effects.
(13) J. Hinze and H. H. Jaffe, *J. Am. Chem. Soc.*, **84**, 540 (1962).
(14) L. C. Allen, E. Clementi, and A. Rauk, *J. Chem. Phys.*, **52**, 4133 (1970).
(15) L. C. Allen, A. Rauk, and K. Mislow, *Angew. Chem.*, **9**, 400 (1970).
(16) The expression for the two-electron stabilization is obtained from perturbation theory with inclusion of overlap; for example, see: L. Salem, *J. Am. Chem. Soc.*, **90**, 543 (1968). The qualitative trend remains the same whether overlap is included or neglected (e.g., see eq 2).
(17) The expression for the four-electron destabilization is obtained by solving the two orbital-four electron interaction problem variationally; for example, see: N. C. Baird and R. M. West, *J. Am. Chem. Soc.*, **93**, 4427 (1971); K. Müller, *Helv. Chim. Acta*, **53**, 1112 (1970). Here inclusion of overlap is necessary to get the correct trend since, when overlap is neglected, ΔE^4 is always zero.
(18) J. M. Lehn, *Fortschr. Chem. Forsch.*, **15**, 311 (1970).
(19) N. D. Epiotis and W. R. Cherry, to be submitted for publication.

Molecular Dynamics of the Hydrogen Iodide and Hydrogen–Iodine Exchange Reactions

R. L. Jaffe, J. M. Henry, and J. B. Anderson*

Contribution from Yale University, New Haven, Connecticut 06520.
Received March 12, 1975

Abstract: A combined phase-space/trajectory study of the hydrogen iodide ($HI + HI \rightarrow H_2 + I_2$) and the hydrogen-iodine ($H_2 + I_2 \rightarrow HI + HI$) exchange reactions was carried out using the semiempirical potential energy surface derived by Raff et al. From a minimum of computation effort the calculations yield overall reaction rates and mechanisms, reactant and product configurations, and energy distributions among reactants and products for thermal reactants at 700 K. The exchange reactions are found to occur through both the C_{2v} trapezoidal and the symmetric linear transition configurations of the potential energy surface used. In reaction of HI + HI via the trapezoidal configuration only stable H_2 and I_2 occur as products. In reaction via the linear configuration the products are primarily stable H_2 molecules and separated I atom pairs with lesser amounts of stable and quasibound I_2 molecules. The calculated overall rate is approximately $\frac{1}{10}$ that from experimental measurements. With adjustment of the relative barrier heights for the two transition configurations to favor the atomic mechanism ($H_2 + 2I \rightarrow HI + HI$) it may be possible to produce agreement with Sullivan's photochemical experiments. The calculated vibrational excitation of reacting HI molecules is in accord with experimental measurements by Jaffe and Anderson. Where directly comparable the results are in agreement with those of a standard quasiclassical trajectory study by Raff et al. However, in the work by Raff et al. a complete statistical investigation of the reactions $H_2 + I_2 \rightarrow HI + HI$ and $H_2 + 2I \rightarrow HI + HI$ was precluded by excessive computer time requirements and the rates of these reactions were underestimated.

Preface

This paper gives a full account of the application of the combined phase-space/trajectory method to the hydrogen iodide and hydrogen-iodine exchange reactions. A summary[1] of results of this study has been published previously. More recent calculations[2] by identical procedures with a modified potential energy surface have also been reported. In these it was found that adjustment of the potential energy surface to promote reaction of HI with HI via a collinear configuration led to reaction products molecular hydrogen [H_2] and either separated iodine atoms [I + I] or molecular iodine vibrationally excited near the dissociation limit [I_2 (hi v)]. It was concluded that slight additional modification of the potential energy surface might favor either set of reaction products.

The validity of the combined phase-space/trajectory method has now been demonstrated for a number of systems[3-7] and is regarded by some as obvious.[8] The calculations reported in the main body of this paper are supplemented by a larger number of conventional trajectories for $H_2 + I_2$ encounters likely to produce reaction as indicated by the combined phase-space/trajectory results. Although there is a large statistical uncertainty in any of the properties calculated for the supplemental set of trajectories, there is essential agreement with the results of the combined phase-space/trajectory method.

*Address correspondence to Department of Chemistry, The Pennsylvania State University, University Park, Pa. 16802.

Table I. Energetically Allowed Reaction Mechanisms

	→	←
Direct reaction		
$HI + HI \rightleftarrows H_2 + I_2$	(R1)	(R1′)
Atomic iodine intermediate		
$HI + HI \rightleftarrows H_2 + I + I$	(R2)	(R2′)
$I + I + M \rightleftarrows I_2 + M$	(R3)	(R3′)
H_2I intermediate		
$HI + HI \rightleftarrows H_2I + I$	(R4)	(R4′)
$H_2I + M \rightleftarrows H_2 + I + M$	(R5)	(R5′)
$I + I + M \rightleftarrows I_2 + M$	(R3)	(R3′)
or		
$H_2I + I \rightleftarrows H_2 + I_2$	(R6)	(R6′)
Chain mechanism		
$HI + H \rightleftarrows H_2 + I$	(R7)	(R7′)
$HI + I \rightleftarrows I_2 + H$	(R8)	(R8′)
Contributing processes		
$I + I + M \rightleftarrows I_2 + M$	(R3)	(R3′)
$H + H + M \rightleftarrows H_2 + M$	(R9)	(R9′)
$H + I + M \rightleftarrows HI + M$	(R10)	(R10′)

I. Introduction

In the development of chemical kinetics over the past century the hydrogen iodide decomposition reaction ($HI + HI \rightarrow H_2 + I_2$) and its reverse, the hydrogen–iodine reaction ($H_2 + I_2 \rightarrow HI + HI$), have played important roles. In one of the first systematic studies of gas-phase reaction rates Bodenstein[9] determined the effects of reactant concentrations and temperature for both reactions. He established that both reactions follow overall second-order kinetics and Lewis[10] later used his data to demonstrate the applicability of Arrhenius' concept of active molecules and the Arrhenius rate expression. Hinshelwood[11] cited the hydrogen–iodine reactions as evidence for the principle of activation by collision. The observed rates were found to be in agreement with the predictions of the simple collision theory of gas reactions.[12] Both Hinshelwood[11] and Kistiakowsky[13] raised the question of the nature of the activation energy and which forms of molecular excitation contribute to the activation process. With the discovery of deuterium the isotope effects on these reactions were examined.[14] One of the early applications of absolute rate theory was the prediction by Wheeler, Topley, and Eyring,[15] with apparent success, of the rate of the hydrogen–iodine reactions. In each of these studies the overall reactions were considered to occur by direct bimolecular mechanisms R1 and R1′ (see Table I). These reactions became "textbook examples" of bimolecular reactions.

More recently, some complexities of the hydrogen–iodine system have been revealed. Benson and Srinivasan[16] and Sullivan[17] showed that a chain mechanism (see Table I) contributes to reaction at temperatures above 600 K and is dominant above 750–800 K. Semenov[18] suggested that the reaction of H_2 and I_2 might occur through the mechanism of I_2 dissociation (R3′) followed by termolecular reaction (R2′). Such a mechanism is kinetically indistinguishable from the direct bimolecular reaction (R1′) if equilibrium is maintained between iodine atoms and molecules. In either case the overall rate is given by an expression first order in H_2 concentration and first order in I_2 concentration. The question of which mechanism dominates the low-temperature reaction was examined by Sullivan[19] in 1967. Using a low-temperature photochemical source of $^2P_{3/2}$ iodine atoms he measured the rate of reaction with molecular hydrogen. Extrapolation of the photochemical rate constants to the higher temperature range of the thermal rate data showed that the former could account for the entire thermal rate. It was thus shown that the dominant mechanism for reaction of H_2 and I_2 below 750–800 K involved I_2 dissociation. It was pointed out by Sullivan that the observed kinetic behavior could be explained by a mechanism involving a loosely bound intermediate H_2I in equilibrium with reactants via reactions (R3′), (R5′), or (R6′) as well as by the termolecular reaction of $H_2 + I + I$ (R2′).

The most accurate overall and specific rate data for the hydrogen–iodine system have been obtained in a series of experiments by Sullivan.[17,20] The measured activation energy for the low-temperature reaction of HI with HI is 43.6 kcal/mol and for the overall reaction of H_2 with I_2 is 40.6 kcal/mol, each corrected for the contribution of the chain mechanism. The reaction of HI with HI to produce $H_2 + I_2$ is endothermic by 3.0 kcal/mol. The dissociation energy of molecular iodine is 36.2 kcal/mol, 4.4 kcal/mol below the activation energy for the overall reaction of H_2 with I_2.

In each of the energetically allowed reaction mechanisms listed in Table I except the chain mechanism the reaction of HI with HI occurs as a direct bimolecular reaction (R1, R2, or R4). The energetically allowed products are $H_2 + I_2$, $H_2 + 2I$, and $H_2I + I$. The reaction has maintained its status as a classic example of a bimolecular reaction although the product distribution was subject to question. The specific energy requirements for activation were investigated by Jaffe and Anderson,[21] who observed that HI and DI in low vibrational states failed to react even at relative translational energies up to two and one-half times the activation energy for reaction. They concluded that rotational or vibrational excitation of the colliding partners is required for an appreciable probability of reaction upon collision.

Several suggestions have been given to explain why an atomic mechanism should be favored over the molecular one. Noyes[22] hypothesized that dynamic effects forbid the bimolecular reaction R1′ and its reverse R1 since the low mass of H_2 allows it to escape before appreciable separation of I atoms can occur. Similar arguments based on momentum conservation can be used to explain the observation that HI and DI in low vibrational states fail to react.

The interatomic forces are of course critical in determining the reaction path. Three transition structures seem most plausible:

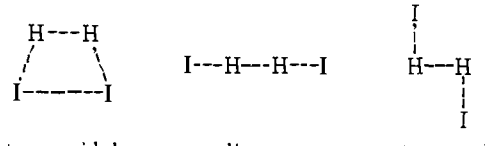

trapezoidal linear staggered

Reaction through the planar trapezoid (C_{2v} symmetry) was initially found by Wheeler, Topley, and Eyring[15] to be the favored pathway for reaction (R1) on an LEP surface. The symmetric linear configuration which appears to be more accessible to $H_2 + 2I$ represents another pathway as does the staggered configuration.

Recent attempts to determine more accurately the potential energy surface and the energetically allowed pathways have been partially successful but the results are not yet definitive. Hoffmann[23] and Cusachs et al.[24] on the basis of simple molecular orbital theory hypothesize that the molecular reaction is energetically not allowed (in the sense of the Woodward–Hoffmann rules) to proceed through a C_{2v} configuration but that other configurations, such as distorted trapezoids, might be more favorable. Raff et al.[25] have calculated a complete valence bond potential energy surface for the H_2I_2 system. On this surface the barriers corresponding to the C_{2v} trapezoid and the symmetric linear configurations have the lowest energies with the trapezoid slightly lower. Both these configurations correspond to the barriers in the minimum energy paths between two HI molecules and hydrogen plus iodine atoms or molecule. Thus, if

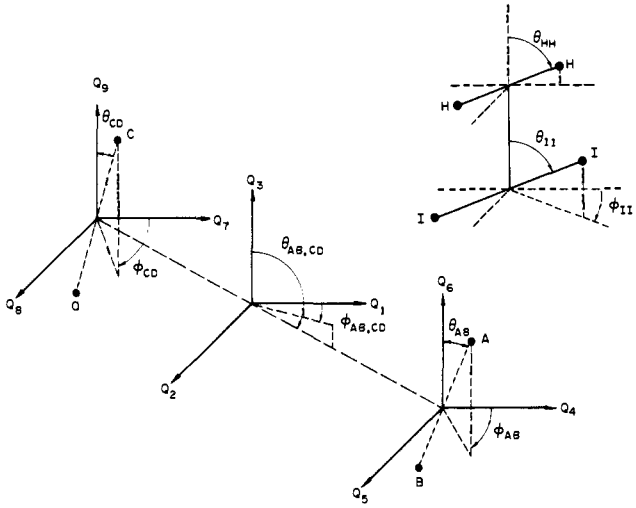

Figure 1. Bimolecular coordinate systems. Inset: arbitrary orientation: $\phi_{H_2,I_2} = 0$, $\theta_{H_2,I_2} = 0$, $\phi_{H_2} = 0$.

their surface is accurate, the only explanation for Sullivan's photochemical experiments is in terms of dynamic effects. Minn and Hanratty[26] have also examined the H_2I_2 valence bond energies but were unable to arrive at barrier heights as low as those of Raff et al.[25] From more accurate calculations Minn and Hanratty find the linear configuration to have a lower energy barrier than the trapezoidal configuration.

Raff et al.[27] have investigated the hydrogen–iodine reactions by means of extensive classical trajectories calculated for the valence bond potential energy surface discussed above. They conclude the direct reaction of H_2 with I_2 is prohibited by dynamic effects and predict that reaction occurs primarily through formation of the H_2I intermediate.

In the present study we have made classical dynamical calculations of reaction trajectories for the hydrogen-iodine system at 700 K. The potential energy surface used is that developed by Raff et al.[27] The combined phase-space/trajectory method,[28,3,5] in which trajectories are sampled from those crossing a surface in phase space dividing reactants and products, has been extended to the four-atom system to minimize the computational effort required. A total of 693 reactive trajectories were obtained with approximately equal statistical weights and representative of reaction in a system with reactants in thermal equilibrium. The method allows the several mechanisms of reaction to be analyzed simultaneously. The results are examined to determine all important kinetic details: the reaction mechanism, the configurations of reactants and products, distributions of energy among reactants and among products, the collision details, and the overall rate. Results are compared with available experimental and theoretical evidence and with the conventional trajectory study of the same system by Raff et al.[27]

In the description which follows we discuss the analysis from the viewpoint of the hydrogen iodide decomposition reaction. The information obtained applies equally to the reaction of hydrogen and iodine to form hydrogen iodide. Determination of the product distribution for the hydrogen iodide decomposition is equivalent to determining the reactant distribution for hydrogen iodide formation when the requirements of microscopic reversibility are considered. For generality, many equations are written in terms of atoms A, B, C, and D with the convention that A and B represent H atoms and C and D represent I atoms.

The distinction between bimolecular and termolecular collisions can be made on the basis of the states of the colliding pairs of atoms. A pair of atoms A and B may exist in any one of four possible types of states. "Bound" molecules AB^b are those pairs with internal energies less than the dissociation energy. Those with energies greater than the dissociation energy can be trapped by the centrifugal or rotational barrier to dissociation. These are "quasibound" (AB^{qb}) and may dissociate in the absence of a third body by tunneling through the barrier. A "dissociative" state (AB^d) occurs for a pair of atoms in close proximity but with internal energy greater than for dissociation by passage over the centrifugal barrier.[29] "Unbound" pairs (A + B) have an internuclear separation greater than that corresponding to the maximum in the centrifugal barrier. The reactions listed in Table I may be specified in further detail by use of these distinctions. In general, we use the conventions that AB includes AB^b and AB^{qb} and that A + B includes AB^d as well as separated atoms.

II. Potential Energy Surface

The potential energy surface for the (H_2I_2) system developed by Raff et al.[25] and used in the present study is based on a simple nonionic valence bond formulation. The system is represented as that of four electrons in the presence of two protons and two I^+ cores. With all overlap and three- and four-center exchange integrals neglected the resulting London expression gives the potential energy in terms of Coulomb and exchange integrals. These are evaluated semiempirically in terms of the lowest singlet $^1\Sigma$ and triplet $^3\Sigma$ potentials using the Heitler–London formulation for diatomic systems. For all diatomic pairs the singlet energies are represented by Morse functions with constants obtained from spectroscopic data. The triplet energies are expressed in analytical forms of the anti-Morse type. For H_2 and I_2 semiempirical approximations are used. The one adjustable parameter, a screening constant for the I^+ cores, is set to give a minimum barrier height for the hydrogen–iodine exchange reaction slightly higher than the observed activation energy. The reader is referred to the original paper by Raff et al.[25] for a complete discussion as well as the analytical expressions and the constants used.

The surface is exact in the limit of separated ground-state diatomic pairs. With one atom removed the barrier heights for the reactions H + I_2 → HI + I and H_2 + I → HI + H are approximately equal to the experimental activation energies for these reactions. Computations of trajectories for these reactions give reasonable agreement with experimental measurements of reaction attributes.[30,31]

For the H_2, I_2 exchange reaction the lowest barriers are those of the C_{2v} trapezoidal configuration (42.04 kcal/mol above the minimum for separated H_2 and I_2) and the symmetric linear configuration (45.60 kcal/mol). The barrier for the staggered configuration lies considerably higher (85.53 kcal/mol). There is a shallow well corresponding to a slightly stable H_2I species when the second I atom is removed to large distances. The locations of the barriers are such that any one of the mechanisms (R1), (R2), (R4) for the exchange reaction listed in Table I is energetically permitted via passage through either the C_{2v} trapezoid or the symmetric linear configuration.

Since the potential energy is a function of the six internuclear distances the surface cannot be described fully by a two- or three-dimensional contour plot. However, using the coordinates R_{H_2}, the internuclear distance between H atoms, R_{I_2} between I atoms, and R_{H_2,I_2} between the centers of masses of H_2 and I_2, together with the angles ϕ_{I_2}, θ_{H_2}, and θ_{I_2} defined in Figure 1, it is found that relatively small variations from $\phi_{I_2} = 0$, $\theta_{H_2} = \pi/2$, and $\theta_{I_2} = \pi/2$ result in increases in potential energy for either of the favored transi-

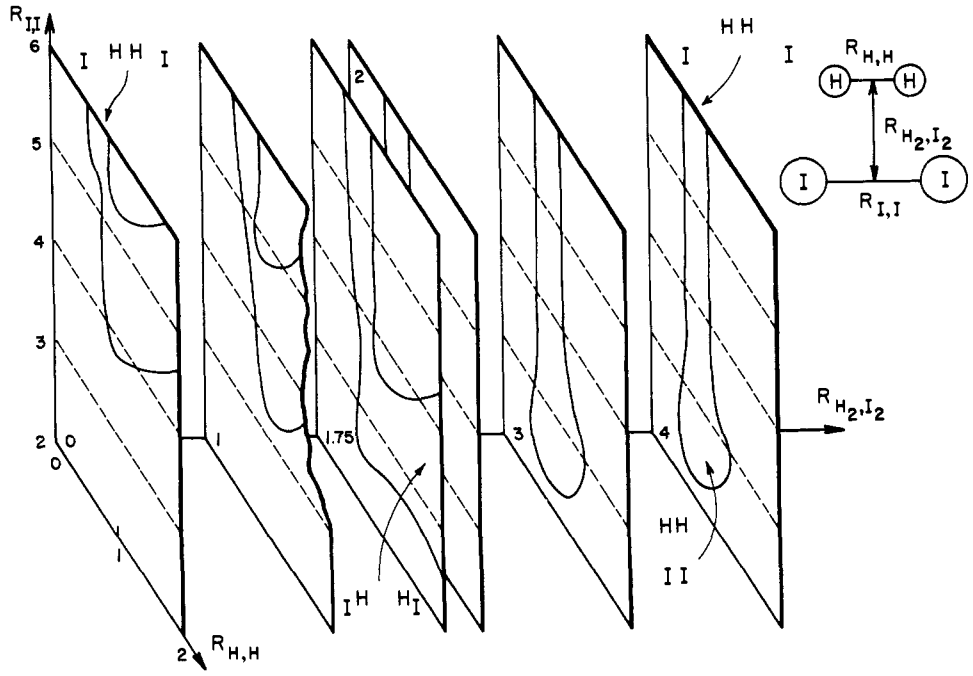

Figure 2. Potential energy surface in (R_{H_2}, R_{I_2}, R_{H_2,I_2}) space. The curves are potential energy contours at 48 kcal/mol relative to the minimum for separated HI molecules. Coordinates in ångströms.

tion configurations. Thus, as an aid to intuition, reaction may be viewed as the motion of a point through the three-dimensional (R_{H_2}, R_{I_2}, R_{H_2,I_2}) space when the angles are specified as above. In Figure 2 the potential energy is mapped as a function of the three distance variables. The locations of the two lowest barriers to reaction are indicated. As shown, the region corresponding to HI + HI occupies the front section (large R_{H_2}, R_{I_2}), $H_2 + I_2$ occupies the rear (large R_{H_2,I_2}; small R_{H_2}, R_{I_2}), and $H_2 + 2I$ is found along the top (small R_{H_2}; large R_{H_2,I_2}, R_{I_2}). The location of the dividing surface separating reactants and products in the six-dimensional configuration space as required for the phase-space/trajectory calculations is discussed in the next section.

An insight into the dynamics of the reaction system can be gained by extension of the sliding mass analogy from two to three dimensions. When the surface of Figure 2 is "diagonalized" to eliminate cross terms in the kinetic energy, the coordinates R_{H_2} and R_{H_2,I_2} are stretched and the three angles between R coordinates become acute angles. The motion of a "floating" mass point under the influence of the potential energy gradients in the resulting R space is then analogous to the behavior of the symmetric planar (H_2, I_2) system with $\phi_{I_2} = 0$, $\theta_{H_2} = \pi/2$, and $\theta_{I_2} = \pi/2$. In view of the importance of rotational motion and asymmetric configurations (see section IV), the utility of the analogy may be limited.

III. Calculation Procedure

A. The Phase-Space/Trajectory Method. Conventional Monte Carlo trajectory calculations may be viewed as an example of the application of the collision theory of gas-phase reactions. Reaction trajectories are determined by solution of the equations of motion for collisions of molecules selected from the distribution of collisions occurring in a mixture of reactants at thermal equilibrium. The path of a trajectory is followed from the initial approach of the reactants until separation of reactants or products occurs.

The combined phase-space/trajectory method is an example of the statistical approach to reaction kinetics. In this method sample trajectories are selected from those crossing the potential energy barrier between reactants and products in a mixture at complete equilibrium. Trajectories are followed forward and backward in time to determine their paths. After elimination of trajectories failing to originate from reactants or proceed to products, a set of trajectories representative of reaction occurring in the absence of products is obtained.

A comparison of the collisional and statistical theories can be made in terms of the phase-space description in which a reaction of N atoms is represented by the motion of a point in the $6N$-dimensional phase space of the coordinates and momenta of the atoms.[32] A canonical ensemble of such systems may be combined to yield a density of points in phase space which may be evaluated for equilibrium conditions. The phase space may be divided into reactant and product regions by a surface of $6N - 1$ dimensions usually located across a saddle point in the potential energy barrier to reaction within the zone of interaction of colliding molecules. In the collisional approach trajectories crossing a surface at the reactant edge of the interaction zone, where equilibrium with separated reactants is assured, are examined to determine their contribution to reaction. In the combined phase-space/trajectory method trajectories are sampled from those crossing the dividing surface within the interaction zone. Thus, it is necessary that the distribution of trajectories in the interaction zone be known under reaction conditions.

The combined phase-space/trajectory method used in this study is based on the principle that in the absence of products the distribution of states in the interaction zone is identical with an equilibrium distribution except that states lying on trajectories originating from products are missing. The question of the distribution in this region was first raised by Marcelin[33] in 1915 and has been the subject of frequent debates ever since. If the assumption of equilibrium for trajectories originating from reactants is correct then the combined phase-space trajectory method and the conventional collisional method will give identical results. The equivalence of the two methods has been demonstrated recently by Anderson[5] for several types of collinear reactions and by Jaffe, Henry, and Anderson[3] in full three-dimensional trajectory calculations for the reaction $F + H_2 \rightarrow HF + H$. Additional theoretical arguments for the prin-

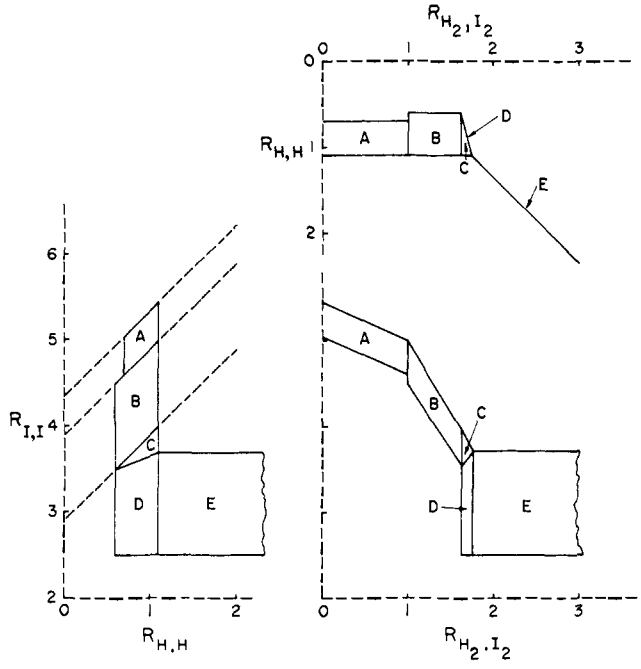

Figure 3. Location of the dividing surface in (R_{H_2}, R_{I_2}, R_{H_2,I_2}) space. Coordinates in ångströms.

ciple of this partial equilibrium with reactants have been given by Keck[28] and are implicit in earlier work by Wigner.[34]

As shown in ref 3 the combined phase-space/trajectory method and the conventional method are not exactly equivalent when the conventional trajectories are calculated using initially quantized reactants. For reactions in which the vibration of light atoms is important significant differences may occur. It is not clear whether including quantum effects at the start of trajectories and omitting them thereafter as in quasiclassical calculations is more correct than omitting quantum effects altogether as in purely classical calculations. Comparisons with exact three-dimensional fully-quantum calculations will be necessary to resolve this question. For the reaction F + H_2 → HF + H the differences between quasiclassical and fully classical treatments are small compared to the uncertainties introduced by an incomplete knowledge of the potential energy surface. This is undoubtedly true for most other reactions.

One major advantage of the combined phase-space/trajectory method is that it gives a much higher overall efficiency in trajectory calculations for reactions in thermal systems. For the (HI + HI) exchange reaction at 700 K the probability of reaction for pairs of molecules with sufficient energy to react is about 1 in 10^6. In a conventional trajectory analysis a set of calculations yielding 1000 reactive trajectories representative of reaction of 700 K would require an excessive computational effort (three billion dollars, at $3 per trajectory examined). With the combined method the effort expended in examining unreactive trajectories is nearly eliminated and the total computation effort is reduced by a factor of nearly 10^6. We should point out that in conventional calculations, many of the trajectories normally examined are selected with total energies somewhat higher than the average of reacting molecules in a thermal mixture and extrapolation to lower energies is utilized in estimating reaction attributes. The computational effort is therefore considerably less than that required to obtain 1000 trajectories representative of reaction in a thermal mixture.

For the general case of a reaction involving N atoms, when the dividing surface is orthogonal to the momentum coordinates, the flux in one direction across the dividing surface for complete equilibrium of reactants and products in terms of the equilibrium rate constant k_e is given in the center-of-mass system by

$$k_e = \frac{g^{\pm}}{\sigma^{\pm}} Q_R^{-1} \int_{\substack{v_n>0 \\ S=0}} \exp\left(-\frac{E}{kT}\right) v_n \beta \prod^{3N-3} dp_j \prod^{3N-4} dq_j \tag{1}$$

in which E is the total energy, q_j and p_j are the conjugate position and momentum coordinates of the atoms, v_n is the velocity in space normal to the dividing surface S, and β relates the differential surface area dS to the position and momentum coordinates. The electronic degeneracy associated with the assumed interaction potential is denoted by $g^{\pm}$ and the effect of particle indistinguishability accounted for by the symmetry number $\sigma^{\pm}$. The partition function Q_R is the product of the classical partition functions per unit volume for the reactants in the center-of-mass system and is defined by

$$Q_R = \frac{g_R}{\sigma_R V^{\nu-1}} \int \exp\left(-\frac{E}{kT}\right) \prod_{j=1}^{3N-3} dp_j \prod_{j=1}^{3N-3} dq_j \tag{2}$$

in which g_R is the product of electronic degeneracies of reactants, σ_R is the product of the symmetry numbers for reactant molecules, V is the volume of the system, and ν is the stoichiometric number of reactant molecules.

In the absence of products the flux across the dividing surface may be less than at equilibrium since not all trajectories crossing the surface from the reactant region originate from the reactants. To obtain the net reaction rate in the absence of products, the conversion coefficient ξ, defined as the fraction of crossing points on S lying on trajectories which originate from reactants and pass directly to the crossing point and eventually to products, must be determined from analyses of trajectories sampled from those crossing the surface at equilibrium. The reaction rate constant k in the absence of products is then given by

$$k = \xi k_e \tag{3}$$

B. The Dividing Surface. To simplify the evaluation of the integral in eq 1 and the sampling of the equilibrium flux for trajectory calculations, the dividing surface was specified in the spherical coordinate system of Figure 1 as a number of sections (indexed k) planar in the (R_{AB}, R_{CD}, $R_{AB,CD}$) space and orthogonal to the six angular configuration variables. The locations were chosen to separate reactants from products at the two saddle points in the barrier to reaction. Five of the sections (A thru E) lie in regions of relatively low potential energy and are accessible to reactants at 700 K. These are shown in Figure 3. Other sections necessary for the complete separation of reactants and products may be placed entirely in regions of higher potential energy and are thus unimportant for reaction at 700 K.

Each of the five sections A thru E is specified by an equation of the form

$$S_k = R_{AB,CD} - a_k R_{AB} - b_k R_{CD} - c_k = 0 \tag{4}$$

with constants and limits of the R's as listed in Table II. The constant β differs for each section and is given by

$$\beta_k = (1 + a_k^2 + b_k^2)^{1/2} \tag{5}$$

The two sections of lowest potential energy are sections A and D, corresponding to the symmetric linear and trapezoidal transition configurations, respectively.

The location of the dividing surface is such that the combination HI + HI occurs on one side of the surface and the

Table II. Parameters for the Dividing Surface

Section (k)	a_k	b_k	c_k	R_{AB}, Å	R_{CD}, Å	R_{ABCD}, Å	^1I_k, 10^{-78} cm^8	V minimum, kcal/mol
A	2.222	−2.222	9.667	0.7–1.1	4.6–5.55	0.0–1.0	2.25	44.87
B	0.645	−0.645	3.516	0.6–1.1	3.50–5.0	1.0–1.643	8.73	43.90
C[a]	0.35	−0.35	2.66	0.6–1.1	3.50–4.01	1.643–1.75	3.48	42.56
D[b]	0.21	0.0	1.519	0.6–1.1	2.5–3.7	1.643–1.75	67.62	41.07
E	1.0	0.0	0.65	1.1–2.9	2.5–3.7	1.75–3.55	1.03	44.15

[a] The region with $R_{AB} < (1.1 - 0.6)/(1.75 - 1.643)R_{ABCD}$ is excluded. [b] The region with $R_{CD} \geq 0.4R_{AB} + 3.26$ Å is excluded.

combinations $H_2 + I_2$, $H_2 + I + I$, and $H_2I + I$ occur on the other. Thus, the overall rate of hydrogen iodine decomposition via (R1), (R2), or (R4) to any of these products (or the formation of HI + HI from any of the combinations) is considered and determination of the product distribution must be made from the results of the trajectory calculations.

C. Rates at Complete Equilibrium. The rate constant k_{e_k} for the equilibrium flux across each section of the dividing surface was determined from eq 1. The total energy is the sum of the potential energy $\mathcal{V}$ (independent of orientation of the four-atom complex but a function of R_{AB}, R_{CD}, $R_{AB,CD}$, ϕ_{CD}, θ_{AB}, and θ_{CD} when $\theta_{AB,CD}$, $\phi_{AB,CD}$, and ϕ_{AB} are arbitrarily specified) and the knetic energy (the sum of the energies associated with each of the nine conjugate momenta $P_{R_{AB}}$, $P_{\theta_{AB}}$, $P_{\phi_{AB}}$, $P_{R_{CD}}$, $P_{\theta_{CD}}$, $P_{\phi_{CD}}$, $P_{R_{AB,CD}}$, $P_{\theta_{AB,CD}}$, and $P_{\phi_{AB,CD}}$). The velocity normal to each section of the dividing surface is

$$v_{n_k} = (P_{R_{AB,CD}}/\mu_{AB,CD} - a_k P_{R_{AB}}/\mu_{AB} - b_k P_{R_{CD}}/\mu_{CD})/\beta_k \quad (6)$$

With these substitutions eq 2 may be integrated analytically over all the momenta and three orientation angles $\theta_{AB,CD}$, $\phi_{AB,CD}$, and ϕ_{AB} to yield for each section

$$k_{e_k} = \frac{g^{\ddagger}}{\sigma^{\ddagger}} Q_R^{-1}(2\mu_{AB,CD}kT)^{3/2}(2\mu_{AB}kT)^{3/2}(2\mu_{CD}kT)^{3/2} \times \pi^4(kT/2)^{1/2}\left\{\frac{1}{\mu_{AB,CD}} + \frac{a_k^2}{\mu_{AB}} + \frac{b_k^2}{\mu_{CD}}\right\}^{1/2} {}^1I_k \quad (7)$$

where ^1I_k is the integral over the remaining coordinates,

$${}^1I_k = 8\pi^2 \int_{S_k=0} e^{-\mathcal{V}/kT} R_{AB,CD}^2 R_{AB}^2 \sin\theta_{AB} \sin\theta_{CD} \times dR_{AB}\, dR_{CD}\, d\theta_{AB}\, d\theta_{CD}\, d\phi_{CD} \quad (8)$$

The integral ^1I_k cannot be obtained analytically because of the complexity of the expression for $\mathcal{V}$. Since the integration is over the surface $S_k = 0$, $R_{AB,CD}$ is a dependent variable determined by R_{AB} and R_{CD}.

The partition function Q_R given by eq 2 may be expressed in terms of the partition functions of the reactant molecules. For separated diatomic molecules AC and BD we have

$$Q_R = (2\pi\mu_{AC,BD}kT)^{3/2} Q_{AC} Q_{BD} \quad (9)$$

where the internal partition functions Q_{AC} and Q_{BD} (diatomic species i) are

$$Q_i = \frac{g_i}{\sigma_i}(2\pi\mu_i kT)^{3/2}\, {}^2I_i \quad (10)$$

with

$${}^2I_i = 4\pi \int_0^{R_i(\max)} \exp(-\mathcal{V}(R_i)/kT) R_i^2\, dR_i \quad (11)$$

The upper limit of integration $R_i(\max)$ is an arbitrary internuclear distance beyond which the diatomic molecules are considered to be separated atoms. With $\mathcal{V}_i$ given by a Morse function ^2I_i must be evaluated numerically.

Table III. Internal Partition Functions at 700 K

Species	σ_i	g_i	V_{ref}[a]	^2I_i, cm^3	Q_i, erg^3 s^3[b]
HI	1	1	M	4.4949×10^{-24}	4.551×10^{-78}
H_2	2	1	M	0.7164×10^{-24}	0.1298×10^{-78}
I_2[b]	2	1	M	17.305×10^{-24}	4428.4×10^{-78}
I_2[qb]	2	1	S		2.72×10^{-73}
I_2[d]	2	1	S		1.45×10^{-73}
(I + I)	2	16	S	V	$4.095 \times 10^{-51} \times V$[c,d]
I	1	4	S		4 (no units)

[a] Zero for potential energy. M = minimum for molecule. S = separated atoms. [b] Defined by eq 10; excludes translational motion of center-of-mass of species; per molecule basis. [c] Units are erg^3 s^3 if V is cm^3. [d] $[(I + I)] = \frac{1}{2}[I]\,[I]\,V$.

Combining eq 7, 9, and 11 gives the equilibrium rate constant for the reaction of AC and BD as

$$k_{e_k} = \frac{g^{\ddagger}}{g_{AC}g_{BD}} \frac{\sigma_{AC}\sigma_{BD}}{\sigma^{\ddagger}} \left(\frac{kT}{8\pi}\right)^{1/2} \frac{{}^1I_k}{{}^2I_{AC}\,{}^2I_{BD}} \times \left\{\frac{1}{\mu_{AB,CD}} + \frac{a_k^2}{\mu_{AB}} + \frac{b_k^2}{\mu_{CD}}\right\}^{1/2} \quad (12)$$

The total equilibrium rate constant k_e is the sum of the individual rate constants k_{e_k} for each section of the dividing surface.

The values of ^1I_k for each surface section were determined for 700 K using an eight-point Gaussian numerical integration technique. The integration was performed over the range ($0 \leq \cos\theta_{AB} \leq 1$, $-1 \leq \cos\theta_{CD} \leq 1$, $0 \leq \phi_{CD} \leq \pi$) thus taking advantage of all symmetry. Parts of some sections k were excluded from consideration when the potential energy in those parts was sufficiently high to make the contribution to the integral negligible. The potential energy was referred to the minimum for separated HI molecules. The results are listed in Table II.

The integrals ^2I_i for H_2, I_2, and HI were evaluated numerically by summing the integrand of eq 11 for 1000 values of R_i in the range of interest. The values obtained, with the potential energy referred to the minimum for each diatomic species, are listed in Table III. The values of the electronic degeneracies, the symmetry numbers, and values of Q_i from eq 10 are also shown. For separated I atoms, treated as a pair of atoms, the potential energy is zero and the integral ^2I_i is equal to the system volume V. The electronic degeneracy for 2I presents special difficulties as discussed in Appendix A, but we have adopted $g_{II} = 16$ for use in the present analysis. The symmetry number associated with the potential energy surface was taken as $\sigma^{\ddagger} = 2$.

For I_2^{qb} and I_2^{d} the partition function Q_i was evaluated with the aid of a transformation to the coordinates P_R, the linear momentum along the internuclear axis and $P_\perp$, the angular momentum. In this notation the internal partition function for a diatomic pair is given by

$$Q_i = \frac{g_i}{\sigma_i} \int e^{-[(P_R^2/2\mu)+(P_\perp^2/2\mu R^2)+\mathcal{V}(R_i)]/kT} \times 8\pi^2 P_\perp\, dP_\perp\, dP_R\, dR_i \quad (13)$$

The integration for I_2^{qb} was carried out by a summation

Table IV. Equilibrium Rate Constants[a]

Surface section k	Specified reactant species: HI + HI k_{ek}, cm³/(mol s)	$H_2 + I_2$ k_{ek}, cm³/(mol s)	$H_2 + 2I$ k_{ek}, 10^{12} cm⁶/(mol² s)
A	0.0105	0.29	0.0146
B	0.0146	0.40	0.0203
C	0.0043	0.12	0.0060
D	0.074	2.03	0.103
E	0.0023	0.063	0.0032
All	0.106	2.90	0.147

[a] Rate constant k_{ek} giving the flux in one direction across the dividing surface for all species in complete equilibrium in terms of the concentrations of the reactants specified.

over small intervals of P_R, $P_\perp$, and R_i including only contributions to the integrand for states with total energy greater than the dissociation energy but less than that of the rotational barrier and with R_i less than that corresponding to the top of the barrier. Similarly, Q_i for I_2[d] was obtained over all states with total energy greater than the rotational barrier and R_i less than that for the top of the barrier. These values are listed in Table III.

Listed in Table IV are the equilibrium rate constants k_{ek} for each section of the dividing surface computed using eq 12. These constants and the sum k_e are shown as calculated for reaction in the forward direction, HI + HI as reactants, and in the reverse direction, $H_2 + I_2$ as reactants. Since the flux across the dividing surface is that for complete equilibrium it includes trajectories leading to (or originating from) all types of iodine pairs (I_2[b], I_2[qb], I_2[d], 2I) and to (or from) the H_2I species.

Using the partition functions listed in Table III the classical equilibrium constants K_{eq} may be calculated for several of the reactions listed in Table I. These were calculated according to

$$K_{eq} = (Q_P/Q_R)\, e^{-\Delta V_0/kT} \tag{14}$$

in which Q_P and Q_R are defined as in eq 2. The constants are listed in Table V together with corresponding values from quantum-mechanical calculations and from experimental measurements. The discrepancies between classical and quantum equilibrium constants suggest limits to the accuracy of classical mechanics in treating these reactions. We should not expect the classical rate constants to be more accurate than the classical equilibrium constants.

D. Selection of Sample Trajectories. Sample trajectories were selected for analysis from the equilibrium flux crossing the dividing surface. For each section trajectories were selected from a distribution with statistical weights given by the integrand of eq 2. In the spherical coordinate system described previously the three orientation angles $\phi_{AB,CD}$, $\theta_{AB,CD}$, and ϕ_{AB} were arbitrarily fixed at 0 and the remaining five position coordinates were selected with statistical weights given by the integrand of eq 9. To accomplish this integrals ^1I_k were evaluated using a procedure in which a subtotal in the summation for the integral was generated for each element of a linear array of the integration steps. A random phase was used repeatedly in locating the eight intervals for each coordinate. Random numbers in the range (0, 1) were matched to the ratios of the subtotal to the total to specify elements in the array and the corresponding coordinates for sample trajectories.

For the momenta the selection was also simplified by specifying $\phi_{AB,CD}$, $\theta_{AB,CD}$, and ϕ_{AB} as 0. In eq 1 the velocity across the dividing surface is dependent on only $P_{R_{AB,CD}}$, $P_{R_{AB}}$, and $P_{R_{CD}}$ and the relevant portion of the integral for each section is

$$M_k = \beta_k^{-1} \int_{v_n>0} \exp\{-(P_{R_{AB,CD}}^2/\mu_{AB,CD} + P_{R_{AB}}^2/\mu_{AB} + P_{R_{CD}}^2/\mu_{CD})/2kT\} \times (P_{R_{AB,CD}}/\mu_{AB,CD} - a_k P_{R_{AB}}/\mu_{AB} - b_k P_{R_{CD}}/\mu_{CD}) \times dP_{R_{AB,CD}} dP_{R_{AB}} dP_{R_{CD}} \tag{15}$$

With a change of variables this can be reduced to an integral of the type

$$M_k \sim \int_{-\infty}^{\infty} e^{-v^2}\, dv \int_{-\infty}^{\infty} e^{-t^2}\, dt \int_0^{\infty} e^{-s^2}\, ds \tag{16}$$

The variables v, t, and s were selected using random numbers N_R in the interval (0, 1) according to

$$v, t = \pm\psi$$
$$\operatorname{erf}\psi = N_R \tag{17}$$

with the sign ± random, and

$$s = \pm(-\ln N_R)^{1/2} \tag{18}$$

The sign ± in eq 18 determines the direction of the trajectory in crossing the surface. With a change to the original variables, $P_{R_{AB,CD}}$, $P_{R_{AB}}$, and $P_{R_{CD}}$ are obtained.

Since the trajectory calculations were carried out using the Cartesian coordinate system and the momenta $P_{\phi_{AB,CD}}$, $P_{\theta_{AB,CD}}$, $P_{\phi_{AB}}$, $P_{\theta_{AB}}$, $P_{\theta_{CD}}$, and $P_{\phi_{CD}}$ and the exponentials involving these momenta could be readily transformed, their selection was made in the Cartesian system. The coordinates used, as for the spherical system, specify the position of the center of mass of AB with respect to CD, of A with respect to B, and of C to D. In the initial orientation with $\phi_{AB,CD} = 0$, $\theta_{AB,CD} = 0$, and $\phi_{AB} = 0$, the initial Cartesian values Q_i^0 are

$$Q_1^0 = 0,\ Q_4^0 = R_{AB}\sin\theta_{AB},\ Q_7^0 = R_{CD}\sin\theta_{CD}\cos\phi_{CD},$$
$$Q_2^0 = 0,\ Q_5^0 = 0,\ Q_8^0 = R_{CD}\sin\theta_{CD}\sin\phi_{CD}, \tag{19}$$
$$Q_3^0 = R_{AB,CD},\ Q_6^0 = R_{AB}\cos\theta_{AB},\ Q_9^0 = R_{CD}\cos\theta_{CD}$$

The conjugate momenta $P_1^0, \ldots, P_9^0$ are then given by

$$P_1^0 = \pm(2\mu_{AB,CD}kT)^{1/2}\psi_i$$
$$P_2^0 = \pm(2\mu_{AB,CD}kT)^{1/2}\psi_i$$
$$P_3^0 = P_{R_{AB,CD}}$$
$$P_4^0 = P_{R_{AB}}\sin\theta_{AB} + P_{\perp_{AB}}\cos\theta_{AB}$$
$$P_5^0 = \pm(2\mu_{AB}kT)^{1/2}\psi_i$$
$$P_6^0 = P_{R_{AB}}\cos\theta_{AB} - P_{\perp_{AB}}\sin\theta_{AB}$$
$$P_7^0 = P_{R_{CD}}\sin\theta_{CD}\cos\phi_{CD} - P_{\perp_{CD}}\cos\theta_{CD}\cos\phi_{CD} - P_{\perp_{CD}'}\sin\phi_{CD}$$
$$P_8^0 = P_{R_{CD}}\sin\theta_{CD}\sin\phi_{CD} + P_{\perp_{CD}}\cos\theta_{CD}\sin\phi_{CD} + P_{\perp_{CD}'}\cos\phi_{CD}$$
$$P_9^0 = P_{R_{CD}}\cos\theta_{CD} - P_{\perp_{CD}}\sin\theta_{CD}$$
$$P_{\perp_{AB}} = \pm(2\mu_{AB}kT)^{3/2}\psi_i$$
$$P_{\perp_{CD}} = \pm(2\mu_{CD}kT)^{3/2}\psi_i$$
$$P_{\perp_{CD}'} = \pm(2\mu_{CD}kT)^{3/2}\psi_i \tag{20}$$

where $\operatorname{erf}\psi_i = N_R$ and the sign ± is random as for eq 17.

Equations 19 and 20 specify completely the sample trajectories crossing the dividing surface and provide the initial conditions for trajectory analysis forward or backward in time to determine their paths.

E. Trajectory Calculations. The trajectories used in the determination of the conversion coefficient and reactant

Table V. Equilibrium Constants at 700 K

Reaction	K_{eq} Quantum[a]	Classical	Exptl[a]	Units[b]
$H_2 + I_2 \rightleftarrows 2HI$	54.3	27.3	53.3	None
$I_2 \rightleftarrows 2I$	2.01×10^{-11}	1.96×10^{-11}	2.01×10^{-11}	mol/cm^3
$H_2 + 2I \rightleftarrows 2HI$	2.71×10^{12}	1.39×10^{12}		cm^3/mol

[a] References 35 and 36. See also ref 20. [b] Unitless if concentrations ratioed to a reference of 1 mol/cm^3.

and product distributions were started on each section of the dividing surface with initial position and momentum coordinates selected as described above. A trajectory was first followed backwards toward HI + HI until it (a) reached the edge of the reactant zone (as indicated by an internuclear distance greater than R_{max}) or (b) recrossed the dividing surface. If the trajectory recrossed the dividing surface it was considered unsuccessful and no further analysis was required. If the trajectory met condition (a) it was followed forward from the initial point on the dividing surface until it (c) reached the edge of the reactant zone or (d) reached the edge of the product zone (also indicated by an internuclear distance greater than R_{max}) regardless of additional surface crossings. Trajectories which met criteria (a) and (d) were termed "successful". These trajectories originated from reactants, passed directly to the chosen crossing point on the dividing surface, and eventually reached products.

The technique is illustrated in Figure 4 for a set of eight trajectories. The initial crossing points selected are indicated by solid circles and the computed section of each trajectory is indicated by a solid line. The dashed line indicates a section not analyzed. Numbers 1, 2, 4, 5, and 6 meet criterion (a) and are subjected to analysis in the forward direction from the initial crossing point. Of these numbers 2, 4, 5, and 6 meet criterion (d). The conversion coefficient is $\frac{4}{8}$ for the overall reaction. The product distribution is $H_2 + I_2$, 1; $H_2 + 2I$, 2; $H_2I + I$, 1.

The analysis of trajectories was made by numerical solution of Hamilton's classical equations of motion. The 18 simultaneous equations were integrated using a fourth-order, modified Adams method[37] with a time step of 2.0×10^{-16} s. The choice of time step led to conservation of total energy to within two parts per thousand for trajectories of average length. The end point limit R_{max} was 6 Å. A sample batch of trajectories with long and complex collisions was repeated with a smaller step size (1.0×10^{16} s) and greater R_{max} (10 Å). In all cases the essential results were the same as for the original trajectories except for small changes in the energy partitioning among reactants or among products. Since errors tend to accumulate during a trajectory calculation, the method of calculating forward and backward from the barrier has the advantage that the errors are smallest in the most sensitive region. The calculations were performed on an IBM 7094/7044 system using the Fortran IV language. Typical computing times were 20–40 s per trajectory.

F. Reactant and Product Analyses. The configurations and energies of reactant and product species were determined for all successful trajectories. The initial determination of atomic or molecular species was made on the basis of internuclear distances. The internal energy and angular momentum about the center-of-mass of each diatomic species were evaluated from the relative motion of the atoms and the Morse interaction potential for the pair. The translational energy of each reactant and product species was computed for the center-of-mass of each species relative to the center-of-mass of the system.

Table VI. Spectroscopic Constants[a]

	H_2	I_2	HI
G_1	4400.26	214.57	2309.5
G_2	−120.81	−0.6127	−39.73
F_{11}	60.839	0.03735	6.551
F_{12}	−3.0176	−0.000117	−0.183
F_{21}	−0.0468	0.0	0.000213
F_{22}	0.0017	0.0	0.000003

[a] Source: H_2, ref 38; I_2, HI, ref 39. All quantities in units of cm^{-1}.

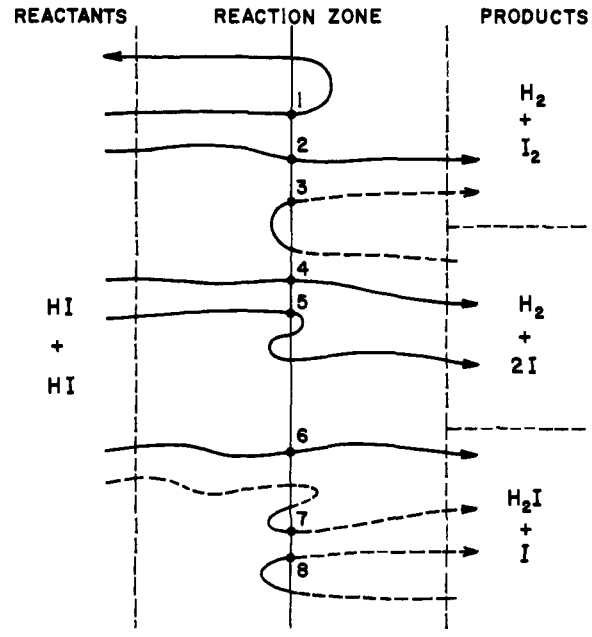

Figure 4. Example of procedure for determining conversion coefficient. Selected crossing point indicated by filled circle. Solid lines represent the examined sections of trajectories.

All H_2 and HI atom pairs occurred with internal energies below the dissociation energy. For I–I pairs it was necessary to determine the type of state occurring (I_2^b, I_2^{qb}, I_2^d, or 2I). For all molecules the distribution of internal energy $E_{v,J}$ between rotational and vibration modes was determined from $E_{v,J}$ and the angular momentum P_J utilizing the spectroscopic term equation,

$$E_{v,J} = \sum_{i=1}^{2} \left\{ G_i(v + \tfrac{1}{2})^i + \sum_{j=1}^{2} F_{i,j}(v + \tfrac{1}{2})^{j-1}[J(J+1)]^i \right\} \tag{21}$$

without restriction to integral quantum numbers v and J. The constants used are listed in Table VI. The vibrational energy E_{vib} and rotational energy E_{rot} were defined by

$$E_{vib} = \sum_{i=1}^{2} G_i(v + \tfrac{1}{2})^i \tag{22}$$

and

$$E_{rot} = \sum_{i=1}^{2}\sum_{j=1}^{2} F_{ij}(v + \tfrac{1}{2})^{j-1}[J(J+1)]^i \tag{23}$$

Table VII. Summary of Trajectory Results

Surface section	No. of trials	Unsuccessful trajectories: Backward path recrossed	Unsuccessful trajectories: Forward path led to reactants	Successful trajectories[a]: Total no.	Successful trajectories[a]: No. with multiple crossings	Products formed[a]: I_2	Products formed[a]: $I_2{}^{qb}$	Products formed[a]: $I_2{}^{d}$	Products formed[a]: 2I
A	332	49	142	141	14	27	15	71	28
				(6.4)		(18)	(25)	(11)	(18)
B	145	42	15	88	4	73	6	8	1
				(6.7)		(8)	(40)	(34)	(100)
C	275	183		92		92			
				(8.5)		(8.5)			
D	496	216	2	278		278			
				(4.0)		(4.0)			
E	101		7	94	10	94			
				(2.7)		(2.7)			
Overall	1349	490	166	693	28	564	21	79	29
				(2.6)		(3)	(22)	(11)	(18)

[a] The percent standard errors are in parentheses.

Table VIII. Conversion Coefficients and Product Distributions

Section	ξ_k	Product distribution: $H_2 + I_2{}^{b}$	Product distribution: $H_2 + I_2{}^{qb}$	Product distribution: $H_2 + I_2{}^{d}$	Product distribution: $H_2 + 2I$
A	0.425	0.192	0.106	0.504	0.198
B	0.607	0.829	0.068	0.091	0.012
C	0.335	1.000			
D	0.560	1.000			
E	0.931	1.000			
All[a]	0.551	0.913	0.018	0.052	0.017

[a] Weighted average.

Table IX. Comparison of Rate Constants

Reaction	Rate constant k at 700 K[a]: Calcd	Rate constant k at 700 K[a]: Exptl[b]
Overall reactions[c]		
$2HI \rightarrow H_2 + I_2/2I$	0.059	0.54
$H_2 + I_2 \rightarrow 2HI$	1.59	29.3
$H_2 + 2I \rightarrow 2HI$	0.82×10^{11}	14.7×10^{11}
Elementary steps[d]		
$2HI \rightarrow H_2 + 2I/I_2{}^{d}$	0.0054	
$2HI \rightarrow H_2 + I_2{}^{b}/I_2{}^{qb}$	0.055	
$H_2 + I_2{}^{b} \rightarrow 2HI$	1.45	
$H_2 + I_2{}^{qb} \rightarrow 2HI$	7.3×10^{7}	
$H_2 + 2I \rightarrow 2HI$	5.5×10^{9}	14.7×10^{11}

[a] Units of $(mol/cm^3)^{-1}\ s^{-1}$ or $(mol/cm^3)^{-2}\ s^{-1}$, as appropriate. [b] From Sullivan.[19,20] HI decomposition rate constant calculated from K_{eq} and k for reverse reaction. [c] Rate constant for reaction by all processes with reactants in thermal equilibrium. Contribution of chain mechanism excluded. [d] Reaction of $H_2 + 2I$ includes $H_2 + I_2{}^{d}$.

We note that the diatomic vibrational levels given by eq 21 agree quite well with spectroscopic measurements for H_2 and HI. For higher levels of I_2 the predicted spacing is much less than the true spacing and the calculated quantum number v is inaccurate. However, the vibrational energies calculated using the above procedure appear reasonably accurate. For I-I pairs the height and location of the centrifugal barrier of the effective potential were calculated as a function of P_J so that the type of state could be determined.

IV. Results

A. General. A total of 1349 trajectories crossing the dividing surface were examined. Of these 490 recrossed the dividing surface in the backward integration toward reactants. The remaining 859 which originated directly from reactants were followed in the forward direction. In this group 166 returned to reactants and 693 were successful in reaching products. For the 166 fully integrated nonreactive trajectories no exchange of the HI partners (i.e., AC + BD $\rightarrow$ AD + BC) was observed. Only 28 successful trajectories exhibited multiple crossings of the dividing surface between reactants and products. For starting points on sections A and B of the dividing surface the full range of iodine species occurred as products, but for starting points on sections C, D, and E only stable iodine molecules were observed. None of the trajectories led to the formation of a stable H_2I complex.

Although the starting points for trajectories were selected with equal statistical weights within each section of the dividing surface, it was impractical to maintain the exact weighting between sections. Because of the large value of k_{eD} relative to k_{eC} or k_{eE} the numbers of trajectories for sections C and E would have been too low to constitute adequate samples. Thus, for the sections with low k_{ek} the number of trajectories examined was higher than required for an exact statistical balance and weighted sums were required in determining the overall reaction properties.

A complete listing of all trajectories in terms of initial crossing point location, additional surface crossings, and product configurations is given in Table VII. The conversion coefficients ξ_i for each section are listed in Table VIII for the overall reaction and for reaction to specific products.

The standard sampling error estimates for ξ_k listed in Table VIII were calculated using the formula

$$\epsilon = ((N_i - n_i)/N_i n_i)^{1/2} \qquad (24)$$

in which ϵ is the fractional error, N_i is the number of trajectories examined, and n_i is the number of successful trajectories found.

B. Rate Constants. The computed rate constants for each of the elementary reactions (R1), (R2), and (R4) and the overall rate constant for hydrogen iodide decomposition by these three reactions are listed in Table IX. Also shown are the rate constants for the reverse reactions (R1′), (R2′), and (R4′) involving each type of iodine pair and H_2I. Since no bound or quasibound H_2I was observed, the upper limit to the transmission coefficient and the standard error were computed with the assumption that each section of the dividing surface contributed one successful trajectory. The partition function for H_2I was not computed; thus, no upper limit for the rate constant of its reaction with I atoms was obtained directly.

For equilibrium between the various iodine species the rate for the overall reaction of H_2 with I_2 via any of the reactions (R1′), (R2′), and (R4′) may be expressed in terms

Table X. Apparent Total Energy Thresholds for HI Production[a]

Section	Threshold (kcal/mol) for H_2 vibrational state, v			
	$v < -0.1$	$-0.1 \leq v \leq 0.1$	$v > 0.1$	$v > 0.9$
	$H_2 + I_2{}^b/I_2{}^{qb} \rightarrow HI + HI$			
A	51.32	50.90	55.79	*b*
B	48.30	52.23	54.95	63.05
C	48.46	50.13	52.54	*b*
D	44.29	45.23	47.34	52.70
E	46.10	47.82	46.35	53.96
	$H_2 + I_2{}^d/2I \rightarrow HI + HI$			
A	48.70	50.53	51.50	*c*
B	53.12	56.55	57.92	*c*

[a] Total energy relative to the minimum for separated H_2 and I_2. Add 2.0 kcal/mol for the reverse reaction relative to the minimum for separated *HI* and HI. [b] No trajectories observed. [c] Not determined.

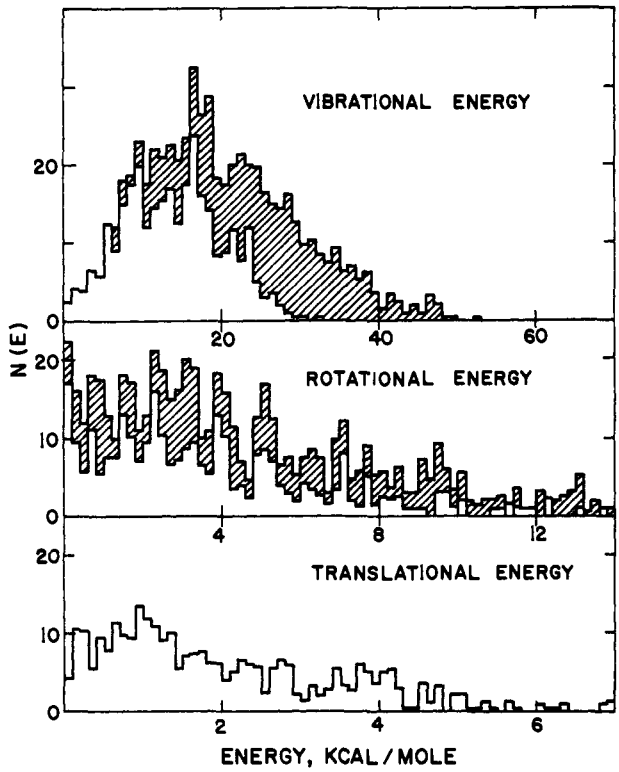

Figure 5. Histograms of HI vibrational, rotational, and total energy for reactive trajectories. Unshaded histograms are for the HI molecule of lower energy in reacting pairs. Shaded are for the molecule with higher energy. Energies in kcal/mol.

of the bimolecular rate constant or the termolecular rates constant k_{ter} defined by

$$d[HI]/dt = 2k[H_2][I_2] = 2kK_D^{-1}[H_2][I]^2 \qquad (25)$$

where $k_{ter} = kK_D^{-1}$ and K_D is the equilibrium constant for dissociation of iodine molecules. Similarly, the rate of the specific reaction (R2′) may be expressed in terms of a termolecular rate constant. These are listed in Table IX.

C. Threshold Energies. A threshold energy is normally defined as the minimum energy required for reaction to occur. This information is not available from the trajectory results, but the "apparent" threshold energy, the minimum energy for which a reactive trajectory was *observed*, provides an upper limit to the true threshold. The minimum barrier height provides a lower limit.

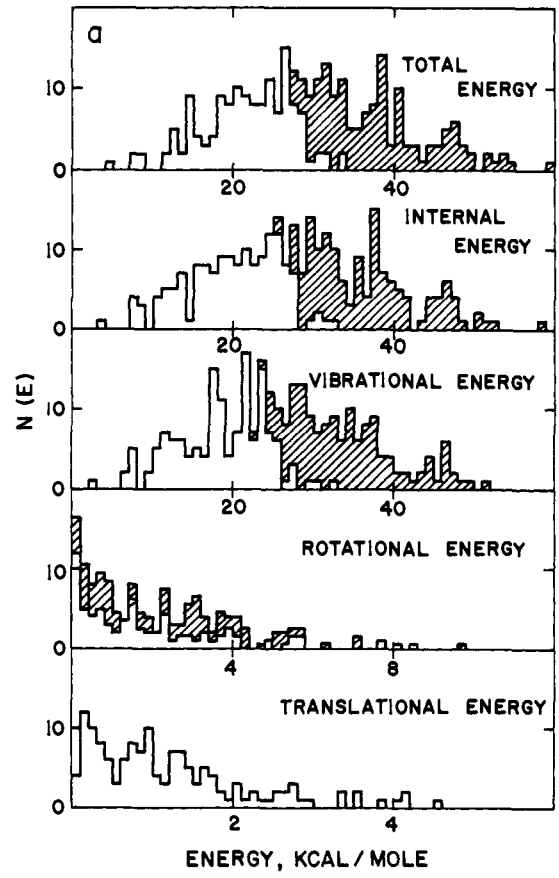

Figure 6. Histograms of HI energies for reactive trajectories with initial crossing points on surface section A. Unshaded/shaded for HI with lower/higher energy.

Table X gives the apparent total energy thresholds for reaction via initial crossing points on each of the sections of the dividing surface. The thresholds are separated into those for the reaction of H_2 and I_2 (bound and quasibound) and of H_2 + 2I (separated and dissociative) with a further subdivision according to the vibrational energy of the H_2 reacting. Thus an approximate threshold for the reaction H_2 ($v = 0$) + $I_2{}^b$ (or $I_2{}^{qb}$) → 2HI may be obtained by picking the reactive trajectory with the minimum total energy from all those with $-0.1 < v_{H_2} < 0.1$. The threshold for the reverse reaction is 2.0 kcal higher since the potential energy reference for reactants (minimum for separated reactants) is lower.

D. Reactants and Product Energy Distributions. Figures 5–11 show histograms of the energy distributions for reactants and products occurring for successful trajectories. Where the distributions are given for reaction through all sections of the dividing surface the proper weighting factors have been used in the summations. In Figure 5 the distribution of total energy (relative to the minimum for separated HI + HI) is shown together with the distribution of total vibrational energy of the pair of reacting HI molecules. Figures 6 and 7 show the distributions of HI energies (total, total internal, total vibrational, total rotational, and translational) for reaction through the most important sections of the dividing surface, sections A and D. Similar plots for H_2 product energies (total, internal, vibrational, rotational, and translational relative to the center-of-mass of all products) are shown in Figures 8 and 9. For iodine products, in Figures 10 and 11, the distributions for molecular iodine ($I_2{}^b$, $I_2{}^{qb}$) and atomic iodine ($I_2{}^d$, 2I) are indicated separately. For separated atoms the potential energy (relative to the minimum) and kinetic energy of motion along the line of

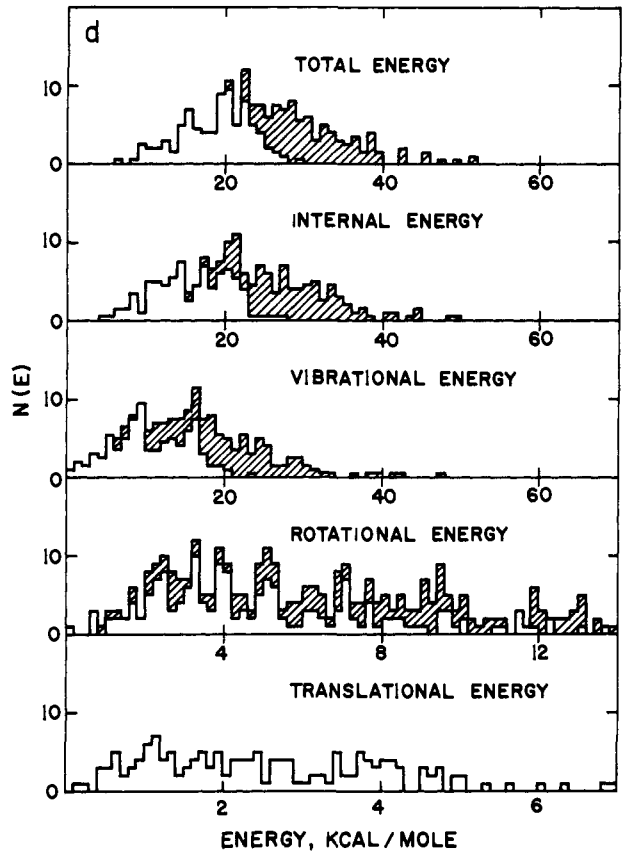

Figure 7. Histograms of HI energies for reactive trajectories with initial crossing points on surface section D.

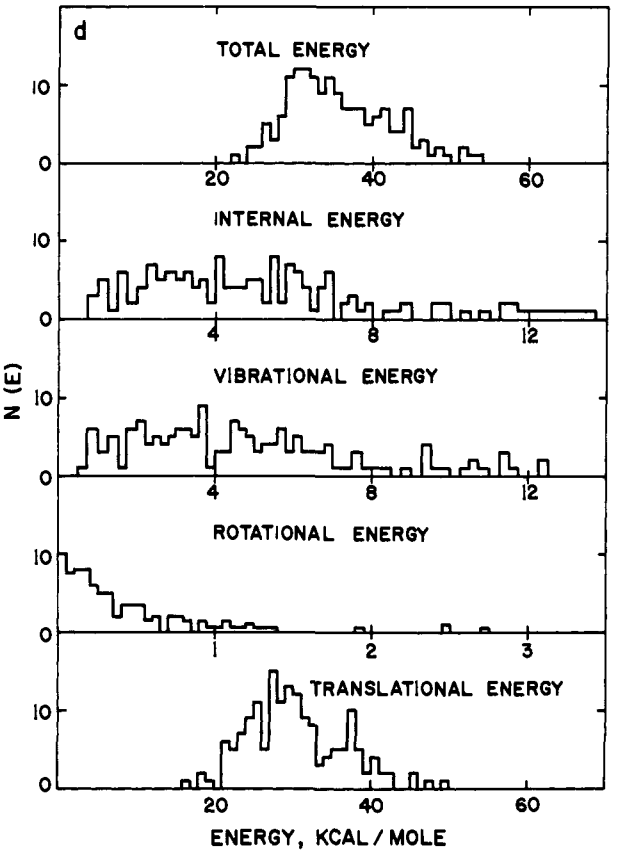

Figure 9. Histograms of H_2 energies for reactive trajectories with initial crossing points on surface D.

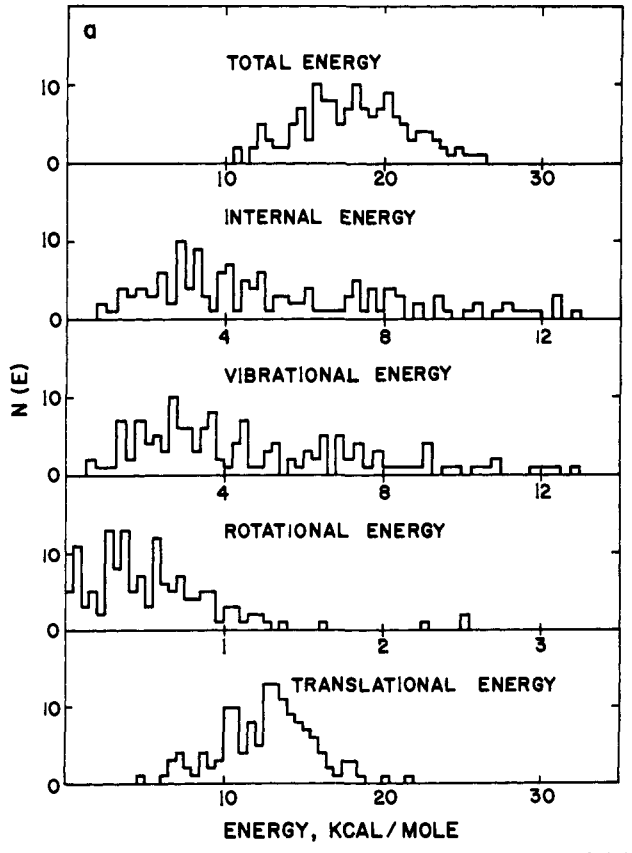

Figure 8. Histograms of H_2 energies for reactive trajectories with initial crossing points on surface A.

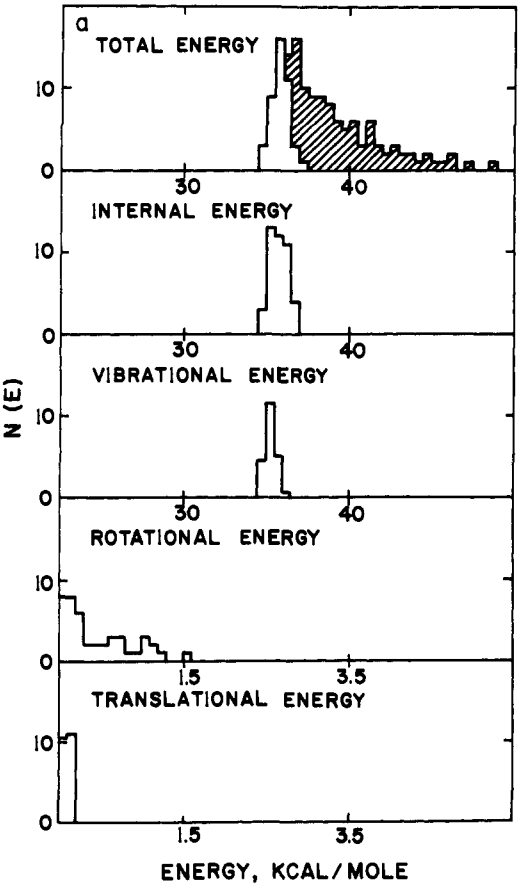

Figure 10. Histograms of I_2 energies for reactive trajectories with initial crossing points on surface A. Unshaded: I_2^b, I_2^{qb}. Shaded: I_2^d, I + I.

Table XI. Average Energies of Reacting HI Molecules (kcal/mol)

Section	$\bar{E}_{tot}$	$\bar{E}_{int}$	$\bar{E}_{vib}$	$\bar{E}_{rot}$	$\bar{E}_{tr}$[a]
A	29.55	28.33	26.14	2.19	1.22
B	29.09	28.11	25.22	2.89	0.98
C	28.13	26.99	23.45	3.54	1.14
D	26.28	23.49	17.08	6.41	2.79
E	26.74	22.79	18.67	4.12	3.95
All[b]	27.01	24.61	19.21	5.40	2.40

[a] One-half the translational energy of relative motion of reacting pairs. [b] Weighted average.

Table XII. Average Energies of H_2 Products (kcal/mol)

Section	$\bar{E}_{tot}$	$\bar{E}_{int}$	$\bar{E}_{vib}$	$\bar{E}_{rot}$	$\bar{E}_{tr}$[a]
A	18.00	5.34	4.76	0.57	12.66
B	22.47	5.12	4.56	0.56	17.35
C	25.80	4.80	4.42	0.39	21.00
D	35.47	5.35	4.97	0.38	30.12
E	40.05	11.42	11.00	0.42	28.63
All[b]	32.09	5.52	5.09	0.42	26.57

[a] Energy associated with H_2 translation relative to center of mass. [b] Weighted average.

Table XIII. Average Energies of I_2/2I Products (kcal/mol)

Section	$\bar{E}_{tot}$[a]	$\bar{E}_{int}$[a]	$\bar{E}_{vib}$[a]	$\bar{E}_{rot}$	$\bar{E}_{tr}$[b]
A[c]	38.48				
B[c]	33.28				
C	27.98	27.82	27.28	0.53	0.17
D	16.11	15.87	15.44	0.43	0.24
E	12.47	12.25	11.82	0.42	0.32
All[d]	20.59				

[a] Energy relative to the minimum for the I_2 molecule. Includes potential energy for dissociated pairs. [b] Energy associated with I_2 translation relative to center-of-mass of all products. [c] Products mainly dissociated: I + I, I_2[d]. [d] Weighted average.

centers is considered as vibrational energy for constructing these figures. Average values of the energies of the participating molecules are listed in Tables XI, XII, and XIII.

The character of the energy distributions can be summarized as follows. Reacting pairs of hydrogen iodide molecules *average* about 59 kcal/mol in total energy for passage through the linear transition configuration and 52 kcal/mol for the trapezoidal configuration. Most of the energy, about 80%, is concentrated in vibration of the HI molecules, with a nearly random distribution of the vibrational energy between the two reacting molecules. For passage through the linear transition region the products are mainly H_2 and separated I atoms or a pair of I atoms in a dissociative state. In this case about 20% of the energy goes into translational motion of the H_2 with respect to the I atoms and 70% into potential and kinetic energy of the I–I pair. For passage through the trapezoid configuration, forming exclusively stable H_2 and I_2 pairs, about 55% of the energy is distributed to translational energy of H_2, 30% to vibrational excitation of I_2 molecules, and 15% to rotation of both molecules.

E. Collision Details. A description of reactive collisions in terms of the motion of the four-atom system about the center-of-mass is, at best, difficult without a full three-dimensional pictorial representation. However, analysis of the changes in interatomic distances and total potential energy provides a reasonably clear picture of the course of reaction. We have examined a small fraction of the 693 reactive trajectories using this method. Figures 12 and 13 show the paths of two trajectories selected as typical of reaction through the linear and trapezoidal configurations, respectively.

Although the rotational and translational energies of the HI molecules are small compared to the combined vibrational energies, the rotation of the HI molecules plays a very important role in the reactive interaction. Detailed examination of the trajectory plots in Figures 12 and 13 shows how reactions occur between two slowly approaching, rotat-

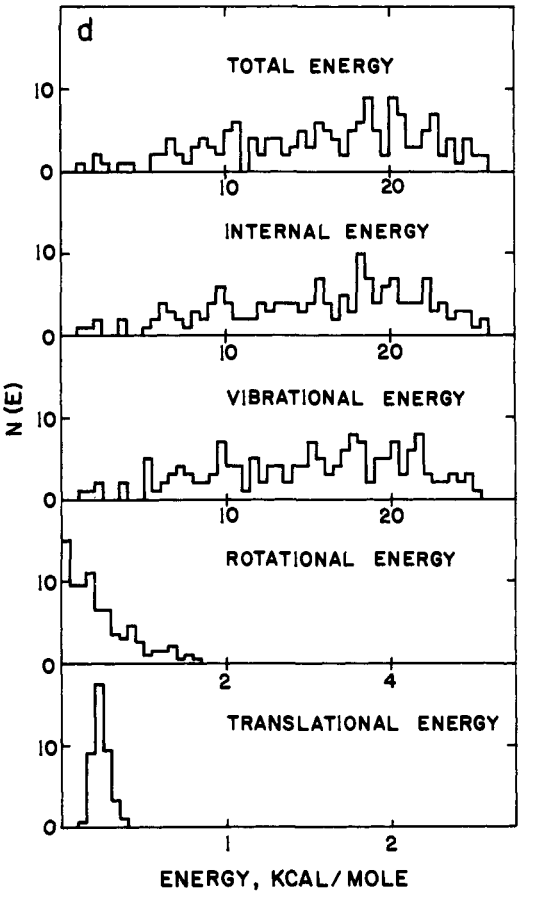

Figure 11. Histograms of I_2 energies for reactive trajectories with initial crossing points on surface D.

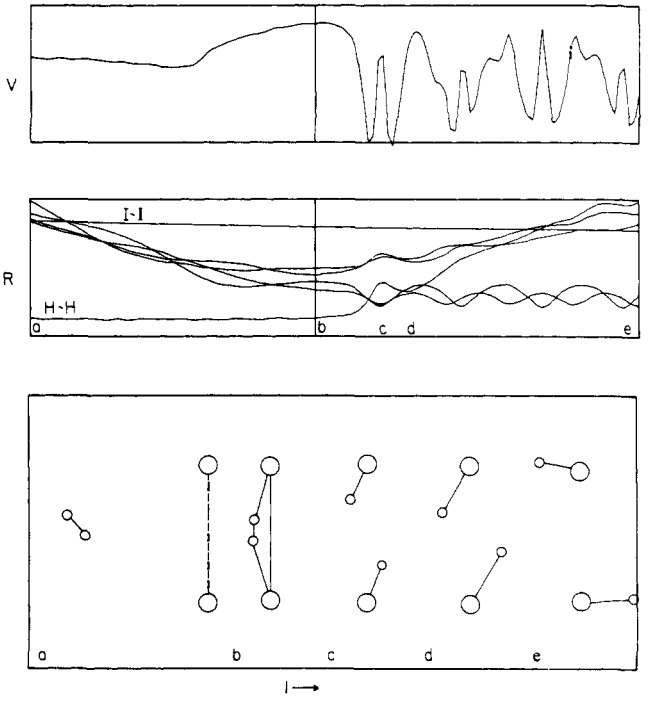

Figure 12. Typical reactive trajectory passing through linear transition region. Potential energy and internuclear distances plotted vs. time. Left edge: $H_2 + I_2$[d]. Right edge: HI + HI. Ball and stick representations for indicated times.

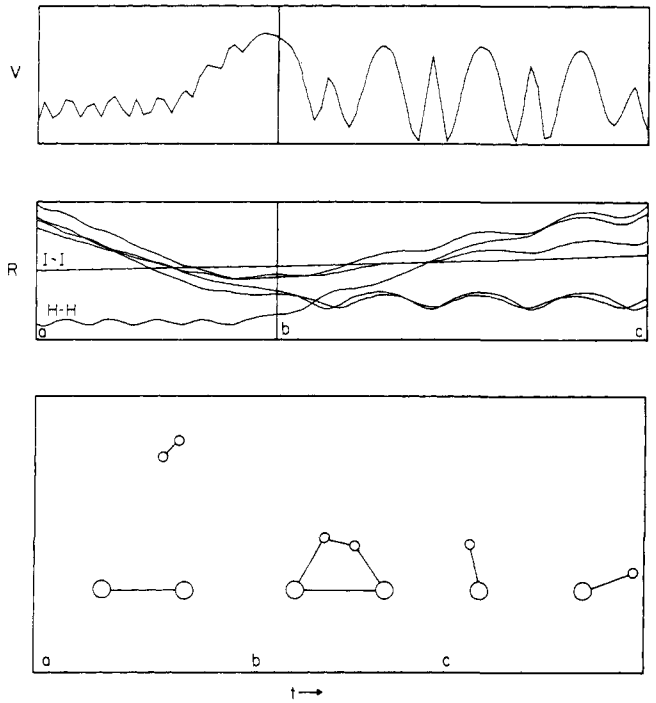

Figure 13. Typical reactive trajectory passing through trapezoidal transition region. Potential energy and internuclear distances plotted vs. time. Left edge: $H_2 + I_2$[b]. Right edge: HI + HI. Ball and stick representations for indicated times.

ing, and vibrating hydrogen iodide molecules. Slow translation coupled with moderately fast rotation provides the opportunity for the two molecules to line up in a trapezoidal or linear configuration. As the hydrogen atoms swing toward each other the interaction tends to distort the vibrations so that the two diatomics stretch in phase. The actual exchange of partners takes place very rapidly with the hydrogen molecule quickly moving away from the iodine atoms.

The nature of the product iodine depends on the I–I separation at the point of closest approach of the hydrogen iodide molecules which in turn is governed by the relative rotational–vibrational phases. If they get close enough together before the hydrogens interact a trapezoidal complex is formed and bound iodine molecules result. If the hydrogens interact at longer I–I distances a linear complex is reached usually resulting in dissociated iodine. Linear complexes tend to be produced if the HI bond lengths are longer (more HI vibration). While the interaction between the two HI molecules acts to synchronize the vibrational phases, this can only be successful if the two molecules are nearly in phase and if the rotational and translational momenta are relatively small.

For reactions occurring via nearly linear configurations both conrotatory and disrotatory motion of the hydrogen atoms around the iodine atoms were observed in nearly equal proportions. Only disrotatory motion was observed in reactive trajectories that proceeded by way of a trapezoidal complex due to a potential energy barrier for bringing a hydrogen atom in between two closely spaced (2.5–3.7 Å) iodine atoms. In the region of closest approach, the H_2I_2 complex was invariably very close to a planar configuration, again due to the lower potential energy for planar configurations.

The trajectory of Figure 12 crossed section A of the dividing surface as a nearly linear complex. From the view point of HI + HI, the two molecules slowly move toward each other, both rotating in the same direction. The individual vibrations and rotations are unperturbed by the neighboring molecule until both hydrogen atoms are in between the iodine atoms, just off the I–I axis. At this point the rotations have been stopped and both HI bonds are increasing as the HI molecules have just passed the inner vibrational turning points. The atomic motions are slowed almost to a halt as the system sits on a potential energy plateau with little kinetic energy before moving down into the hydrogen–iodine valley as the products separate. In this case the products are $H_2 + I_2$[d]. In the reverse direction, the reaction can be pictured as a hydrogen molecule making a rapid broadside approach to a highly separated I_2[d]. As the H_2 nears, it is slowed down until, very close to the iodine, it reorients itself so that the H–H and I–I bonds are parallel and nearly coaxial. This transient complex rapidly decomposes into two vibrationally excited hydrogen iodide molecules which very slowly move apart.

In the trajectory shown in Figure 13 a distorted trapezoidal configuration was assumed by the H_2I_2 system at the point of closest approach. Here the iodine atoms were too close together to permit the hydrogen atoms to be inserted between them either by broadside attack from the $H_2 + I_2$ direction or by the disrotatory motion of the hydrogen atoms around the iodines (from HI + HI). In the latter case a bound iodine molecule was formed. From the direction of $H_2 + I_2/2I$ the nature of the collision complex seems to be governed mainly by the separation of the iodine atoms. In the case of HI + HI collisions, the rotational phase appears to be the determining factor in whether a linear or trapezoidal complex is formed.

Of the 1349 trajectories computed, 15 involved very long interaction times in which the HI molecules remained in close proximity, vibrating and rotating, during the integration from the dividing surface toward reactants. The HI molecules retained their diatomic identities during this process and no exchange of hydrogen–iodine partners occurred. In several cases these trajectories were terminated at 5000 time steps (10^{-12} s) before complete separation took place.

Plots such as those of Figures 12 and 13 showed no indication of the formation of H_2I either as a stable product or as a transitory species. The high kinetic energy of the H_2 leaving the I_2 pairs is an indication that such a species is unlikely as a reaction product.

V. Discussion

A. General. The results indicate that for the potential energy surface employed the contributions of both reaction paths, through the linear and through the trapezoidal configurations, are important. Reaction through the trapezoidal configuration is not prohibited by constraints imposed by conservation of momentum as suggested by Noyes. The conversion coefficient for the reaction of HI + HI to $H_2 + I_2/2I$ is nearly the same for section A (linear) and section D (trapezoid) of the dividing surface. The uncertainty in the relative heights of the barriers to reaction for these two transition configurations is at least 5 to 10 kcal/mol. Since a change ΔE in barrier height of 5 kcal/mol produces a change in rate by a factor of about $\exp(\Delta E/kT) \simeq 35$, the uncertainty in barrier heights results in complete uncertainty as to the main route of reaction. The width of the saddle area (i.e., the size of the low-energy region in the five-dimensional dividing surface in configuration space) and its orientation also affect the importance of each path. These effects favor the linear configuration over the trapezoidal configuration by a factor of 3 which is offset by a factor of 13 for the 3.6 kcal/mol difference in barrier heights with the net result that about ¾ of the observed reaction occurs through the trapezoidal region. Dynamic effects are not

manifested by a low-conversion coefficient for either reaction and the relative barrier heights are crucial in determining the preferred path.

For reaction through the trapezoidal configuration, the observed iodine products consist solely of stable I_2 molecules. Reaction through the linear configuration produces the full range of iodine products but favors the dissociative states I_2^d and separated atoms I + I. It is not clear whether the distribution of iodine products formed via the linear configuration is sensitive to the fine details of the potential energy surface. It seems likely that a slight modification of the surface in the region of the linear transition configuration could shift the product distribution entirely one way or the other (toward stable I_2^b or toward dissociative pairs I_2^d and I + I). It seems unlikely that a minor modification of the surface along the path through the trapezoidal configuration could alter the iodine product distribution for reaction via that path. The average internal energy of the I_2 molecules produced via section D was only 15.87 kcal/mol.

B. Comparison with Experimental Results. The information available from experiments on the H_2, I_2 exchange reaction consists of a body of overall rate data for forward and reverse reactions in thermally equilibrated systems, Sullivan's rate data for the overall reaction $H_2 + I + I \rightarrow HI + HI$ in a thermal mixture, and the observation by Jaffe and Anderson[21] that the cross section for the reaction HI + DI → HD + I_2/2I is low for translationally energetic collisions.

The rate constant for the overall reaction HI + HI → I_2/2I determined from the weighted sum of the rates for each section of the dividing surface is 0.059 cm^3/(mol s), a factor of 9 lower than the experimental rate constant, 0.54 cm^3/(mol s), reported by Sullivan.[20] Similarly, for the reverse reaction (overall, with equilibrated reactants, H_2 + I_2) the calculated rate constant is 1.59 cm^3/(mol s), a factor of 18 lower than the experimentally measured constant, 29.3 cm^3/(mol s).

The calculated termolecular constant for the specific elementary reaction $H_2 + I + I \rightarrow HI + HI$ is 5.5×10^9 $cm^6/(mol^2\ s)$ at 700 K. This may be compared with Sullivan's[19] rate data for the same overall reaction extrapolated from 418–520 to 700 K giving a rate constant of 1470×10^9 $cm^6/(mol^2\ s)$. Sullivan's experiments do not distinguish between reactions R2′ ($H_2 + I + I \rightarrow HI + HI$) and R5′ and R4′ (reaction via H_2I), but since the present results indicate the direct termolecular reaction (R2′) is preferred to the routes involving H_2I as an intermediate, the measured rate appears to be that of reaction R2′.

The calculated rates are in agreement with the experimental rates within the uncertainty introduced by incomplete knowledge of the true potential energy surface. Raising the barrier for the trapezoidal configuration by ~5 kcal/mol or more and lowering the barrier for the linear configuration by ~6 kcal/mol would produce good agreement for the overall rate constants and might give accord with Sullivan's measurements for reactions of I atoms. The rate constant for each surface section could also be altered by varying the "widths" of each saddle region without changing barrier heights. A combination of changes in barrier heights and shapes is probably necessary to achieve exact agreement with the experimental activation energy and frequency factor.

Conclusions regarding the necessity for vibrational excitation of HI reactants apply to reactions producing the full range of iodine products. The observation of substantial vibrational excitation of HI molecules (averaging 15 to 25 kcal/mol each) undergoing reaction is in accord with the conclusion of Jaffe and Anderson[21] that little or no reaction occurs without internal excitation. This result is due to the masses of the atoms and the general features of the potential energy surface for each of the reaction paths and we expect that minor variations of the surface would have little effect.

C. Comparison with Results of Raff et al. In their investigation of the reactions of the hydrogen–iodine system by trajectory analysis, Raff et al.[27] used the same potential energy surface used in the present study. Although the conclusions of the two studies are in agreement on several points, the major conclusions of our study contradict those of Raff et al. Regardless of the agreement or disagreement with experimental measurements the two studies should be in agreement with each other. We find the overall reaction $H_2 + I_2 \rightarrow 2HI$ at 700 K proceeds primarily through the reactions $H_2 + I_2 \rightarrow 2HI$ and $H_2 + I + I \rightarrow 2HI$. Raff et al. find these reactions to be slow and conclude that reaction occurs primarily through the H_2I intermediate by $H_2 + I_2^d \rightleftarrows H_2I^b + I$, $H_2I^b + I \rightarrow 2HI$. We find the direct reaction $H_2 + I_2 \rightarrow 2HI$ to occur at a rate within a factor of 20 of Sullivan's measured rates. Raff et al. state, "The overall rate of such processes is predicted to be five orders of magnitude lower than the experimental values reported by Sullivan."

Using the standard trajectory method Raff et al. investigated the following processes to determine reaction cross sections at several translational energies:

$$H_2 (v = 0) + I_2 (v = 0) \rightarrow HI + HI \quad (P1)$$

$$H_2 (v = 1) + I_2 (v = 0) \rightarrow HI + HI \quad (P2)$$

$$H_2 (v = 2) + I_2 (v = 0) \rightarrow HI + HI \quad (P3)$$

$$H_2 (v = 3) + I_2 (v = 0) \rightarrow HI + HI \quad (P4)$$

$$H_2 (v = 0) + I_2 (v > 0) \rightarrow HI + HI \quad (P5)$$

$$H_2 (v = 1) + I_2 (v > 0) \rightarrow HI + HI \quad (P6)$$

$$H_2 (v = 2) + I_2 (v > 0) \rightarrow HI + HI \quad (P7)$$

For processes P1, P2, P3, and P4 they found translational energy thresholds of about 52, 38, 36, and 27 kcal/mol with rotational states averaged at 738 K. These correspond to total energy thresholds (including 2 kcal/mol rotational energy and zero-point energy of 6.5 kcal/mol) of 60, 59, 67, and 69 kcal/mol, respectively. Comparisons of the calculated rate constants for (P1), (P2), (P3), and (P4) with the experimental data showed these processes to be a factor of 10^5 too slow to account for the measured reaction rates. Since we find no I_2 with vibrational excitation as low as $v = 0$ (0.31 kcal/mol) and only a small fraction with $v < 10$ as a product of HI decomposition (or as a reactant in HI production), there is no disagreement for processes P1 to P4.

Raff et al. were prevented by excessive computer time requirements from complete statistical investigations of processes P5, P6, and P7, but they determined energy thresholds for reaction of H_2 ($v = 0$), H_2 ($v = 1$), and H_2 ($v = 2$) with I_2 having vibrational excitation of 33.8, 30.2, and 18.9 kcal/mol, respectively. Total energy thresholds of 73–77 kcal/mol (67–71 kcal/mol excluding zero-point energies) for process P5 and 59–63 kcal/mol (53–57 kcal/mol excluding zero-point energies) for processes P6 and P7 were reported and it was concluded these processes could make only a small contribution to the rate of HI production. Our results for process P5 differ markedly. As shown in Table X we find a total energy threshold of 45 kcal/mol for process P5, about 25 kcal/mol lower than Raff et al. For processes P6 and P7 we find little contribution to the overall rate and a total energy threshold of 53 kcal/mol for H_2 ($v > 0.9$),

6-10 kcal/mol lower than Raff et al., but in approximate agreement.

Raff et al. investigated more than 2500 collisions of the type $H_2 + I_2^d \rightarrow$ products and found no hydrogen iodide produced except when statistically improbable linear or nearly linear trajectories were specified. We find I_2^d to be a product of HI decomposition (and contributor to HI formation) in small but significant amounts.

On the basis of further calculations Raff et al. found that H_2I^b is formed rapidly in mixtures of H_2 and I_2 and can be assumed to be present in essentially equilibrium concentrations. Although no reaction of H_2I^b with I atoms to produce HI + HI was observed for statistically chosen collisions, they found that the reaction could occur in collinear collisions with a total energy threshold sufficiently low to account for the production of hydrogen iodide in thermal systems. Raff et al. predict the major fraction of HI from the overall reaction of H_2 with I_2 is produced via the intermediate H_2I^b. We find no H_2I^b contributing to HI production.

The dividing surface was located such that (H_2I + I), (H_2 + I_2), and (H_2 + 2I) occurred on one side and (HI + HI) on the other. Thus, the exchanges between (H_2I + I), (H_2 + I_2), and (H_2 + 2I) examined by Raff et al. were not investigated in the present study.

The major points of disagreement are in regard to (a) the total energy threshold and rate for process P5, the reaction of H_2 ($v = 0$) with I_2 ($v > 0$), and (b) the rate of reaction of H_2I^b with I atoms to produce HI. In both cases the conclusions of Raff et al. were made on the basis of incomplete statistical investigations and are thus subject to further inquiry.

We have computed a large number of trajectories for the process P5 using the conventional Monte Carlo trajectory method. Reaction was observed for total energies well below the threshold reported by Raff et al. and our estimate of reaction cross section gives values consistent with the overall rate determined by the combined phase-space/trajectory analysis. Details are reported in Appendix B.

D. The Combined Phase-Space/Trajectory Method. With this study we have demonstrated the feasibility of a complete statistical trajectory study of a complex four-body reaction using the combined classical phase-space/trajectory method. A total of 693 reactive trajectories with approximately equal statistical weights for thermal reactions were obtained without the necessity of extensive calculations of unreactive trajectories. As noted previously the computation effort required to obtain these results by a standard trajectory analysis is prohibitive and has heretofore prevented such an analysis.

We note that the trajectory study of the same reaction system by Raff et al.[27] produced no reactive trajectories with statistical significance for the hydrogen–iodine exchange reactions. The excessive cost of the standard method led to an incomplete investigation of several important reaction processes which apparently resulted in erroneous conclusions regarding the primary mechanism for reaction.

The accuracy of the method in treating real systems is, of course, limited by the accuracy of the potential energy surfaces available and by the use of classical mechanics. In the present case the results show the necessity for a more accurate surface in determining the barrier heights for two different transition configurations. Thus far, the comparisons between classical and quantum treatments for much simpler systems are encouraging in that the classical treatments appear to be adequate for predicting the major reaction attributes.

Acknowledgment. We are indebted to R. K. Preston, R. J. Cross, J. B. Fenn, J. C. Keck, J. C. Polanyi, and R. N. Porter for many valuable discussions. Financial support from the National Science Foundation is gratefully acknowledged.

Appendix A. Effect of Degenerate Electronic States

In treating the H_2, I_2 reaction system it is necessary to consider all the potential energy surfaces on which reaction can occur and the possibility of electronic transitions between surfaces. In the present study the trajectories were calculated for electronically adiabatic collisions occurring on the ground-state potential-energy surface. Although the ground states of the reactants HI + HI and the products H_2 + I_2 are nondegenerate and connect directly with the ground-state potential-energy surface used, the ground state of I is fourfold degenerate and the ground state of the system H_2 + I + I does not necessarily connect with that of the potential energy surface.

The ground state of HI is the nondegenerate $^1\Sigma$ state. The next higher state $^2\Pi$ lies 7.7 eV higher and may be neglected for reaction at 700 K. Similarly, the ground states of H_2 and I_2 molecules are both $^1\Sigma$ and are separated by 11.4 and 1.47 eV from the next higher states. The lowest electronic configuration for atomic iodine is the ^2P state which is split by spin–orbit coupling into a fourfold degenerate $^2P_{3/2}$ state and a doubly degenerate $^2P_{1/2}$ state. The $^2P_{3/2}$ state is the ground state and the $^2P_{1/2}$ state lies about 1 eV higher. For other halogens the separation is considerably less and reactions of the $^2P_{1/2}$ state must be considered (e.g., F + H_2), but for iodine it is assumed that the $^2P_{1/2}$ state may be neglected.

In the recombination of ground-state iodine atoms the fourfold degeneracy of each atom leads to a 16-fold degeneracy for the I + I pair. Since the ground state I_2 molecule is nondegenerate, only one of the 16 states of I + I can lead to I_2 by an adiabatic process. The possibility of nonadiabatic behavior has been considered by several workers. Wigner[40] noted that weakly bound excited states might be formed and subsequently lead to the $^1\Sigma$ ground state by radiative decay. If the four mildly attractive $^3\Pi$ states lead to the $^1\Sigma$ state by rapid transitions, spontaneous or induced by the presence of a third body, the statistical degeneracy factor would be $5/16$. Bunker[41] argues that the degeneracy factor must be close to $1/16$, possibly as large as about $1/8$.

Appendix B. Limited Standard Trajectory Analysis of H_2 + $I_2 \rightarrow$ HI + HI

We have previously reported[42] the results of a limited standard trajectory analysis of the reaction H_2 ($v = 0$, $J = 1$) + I_2 ($v = 40$, $J = 80$) $\rightarrow$ HI + HI. This combination places 6.2 kcal/mol in H_2 vibration, 0.2 kcal/mol in H_2 rotation, 21.2 kcal/mol in I_2 vibration, and 0.6 kcal/mol in I_2 rotation. Because of the high moment of inertia of I_2 the value $J = 80$ does not indicate significant rotational excitation. Reaction was found to occur with a translational energy as low as 20.2 kcal/mol corresponding to a total energy of 48.4 kcal/mol (including zero-point energies). This is 25–29 kcal/mol below the threshold estimated by Raff et al. for their reaction (M4), H_2 ($v = 0$) + I_2 ($v > 0$) $\rightarrow$ HI + HI.

Calculations similar to those reported in ref 42 were carried out for the combination H_2 ($v = 0$, $J = 1$) + I_2 ($v = 20$, $J = 80$). In these we also found reaction to occur at a total energy as low as 48.4 kcal/mol.

The overall rate constant may be estimated from standard trajectory calculations with the I_2 vibrational energy $E_{vib}(I_2)$ and the translational energy E_{tr} chosen according to an importance sampling method making use of information supplied by the combined phase-space/trajectory study, i.e., the energy for reaction is supplied mainly by the

Table XIV. Results for H_2 ($v = 0, J = 1$) + I_2 ($v > 0$) at 700 K

Traj no. (reactive)	W	f	$E_{vib}(I_2)$, kcal/mol	E_{tr}, kcal/mol	$10^{16}e^{-W}$
106	31.72	0.82	7.9	36.2	167.6
137	36.34	0.88	6.1	44.5	1.7
427	32.55	0.61	17.6	27.6	73.1
453	34.84	0.75	12.1	36.3	7.4
637	35.73	0.83	8.4	41.2	3.0
683	35.05	0.87	6.3	42.4	6.0
738	31.64	0.74	11.4	32.5	181.5
878	33.21	0.58	19.4	26.8	37.8
900	34.97	0.79	10.2	38.4	6.5
1008	31.90	0.58	18.6	25.7	140.0
1092	33.68	0.62	17.8	29.0	23.6
1110	33.76	0.81	8.9	38.0	21.8
1119	35.13	0.85	7.3	41.5	5.5
1129	33.51	0.52	22.4	24.2	28.0
1138	35.73	0.74	12.9	36.8	3.0
1159	31.85	0.54	20.4	23.9	147.1
1209	31.27	0.82	7.3	35.6	262.8
1466	34.30	0.83	8.1	39.6	12.7
1874	34.57	0.79	10.1	38.0	9.7
1897	34.64	0.52	23.1	25.0	9.0
1933	33.73	0.80	9.4	37.5	22.5
1951	32.96	0.81	8.7	37.1	48.5
2028	31.75	0.69	13.7	30.5	162.6
2122	35.62	0.88	5.9	43.6	3.4
2157	36.40	0.84	8.1	42.5	1.6

sum of $E_{vib}(I_2)$ and E_{tr}. Approximating the distribution function for $E_{vib}(I_2)$ by $\exp(-E_{vib}(I_2)/kT)$ we obtain:

$$k = \left(\frac{8kT}{\pi\mu}\right)^{1/2} \int\int e^{-E_{vib}(I_2)/kT} e^{-E_{tr}/kT} \times S_r \frac{E_{tr}}{kT} \, d\frac{E_{tr}}{kT} \, d\frac{E_{vib}(I_2)}{kT} \quad (26)$$

or

$$k = \left(\frac{8kT}{\pi\mu}\right)^{1/2} \frac{\pi}{6} \int\int\int e^{-W} P_r \, db^2 \, dW^3 \, df^2 \quad (27)$$

where $W = (E_{tr} + E_{vib}(I_2))/kT$ and $f = (E_{tr}/kT)/W$. Since the vibration of I_2 is anharmonic the contribution of the higher vibrational states to the rate is underestimated by eq 27.

To estimate the rate constant given by eq 27 for the overall reaction at 700 K the third set of standard trajectories was computed with starting points selected as suggested by eq 27. The impact parameter was chosen as b^2 in the range 0 to 0.25 Å^2, the term W^3 in the range corresponding to $(41.0)^3$ to $(51.0)^3$ (kcal/mol)^3, and f^2 in the range of $(4/9)^2$ to $(8/9)^2$. The H_2 molecule was specified as $H_2(0, 1)$. Other initial conditions were selected from the distribution at 700 K. Of the 2200 trajectories calculated 25 led to reaction. Details of the reactive trajectories are listed in Table XIV. The rate constant estimated from eq 27, integrated over the indicated ranges of b^2, W^3, and f^2, is $k \simeq 1.9 \pm 0.8$ (mol/cm^3)$^{-1}$ s^{-1} which may be compared with the value $k = 1.59$ (mol/cm^3)$^{-1}$ s^{-1} given by the combined phase-space/trajectory study.

References and Notes

(1) J. M. Henry, R. L. Jaffe, and J. B. Anderson, *Chem. Phys. Lett.*, **20**, 138 (1973).
(2) J. B. Anderson, *J. Chem. Phys.*, **61**, 3390 (1974).
(3) R. L. Jaffe, J. M. Henry, and J. B. Anderson, *J. Chem. Phys.*, **59**, 1128 (1973).
(4) R. L. Jaffe and J. B. Anderson, *J. Chem. Phys.*, **54**, 2224 (1971).
(5) J. B. Anderson, *J. Chem. Phys.*, **58**, 4684 (1973).
(6) R. N. Porter, D. L. Thompson, L. M. Raff, and J. M. White, *J. Chem. Phys.*, **62**, 2429 (1975). (This paper also reports results of an incorrect combined phase-space/trajectory analysis. These should not be confused with the results of the corrected calculations reported in Table VIII of the paper.)
(7) J. B. Anderson, *J. Chem. Phys.*, **61**, 2446 (1975).
(8) I. Mayer, *J. Chem. Phys.*, **60**, 2564 (1974).
(9) M. Bodenstein, *Z. Phys. Chem. (Frankfurt am Main)*, **13**, 56 (1894); **22**, 1 (1897); **29**, 295 (1899).
(10) W. C. McC. Lewis, *J. Chem. Soc.*, **113**, 471 (1918).
(11) C. N. Hinshelwood, "The Kinetics of Chemical Change in Gaseous Systems", Oxford University Press, Oxford, England, 1926, p 52.
(12) P. Langevin and J.-J. Rery, *Radium (Paris)*, **10**, 142 (1913).
(13) G. B. Kistiakowsky, *J. Am. Chem. Soc.*, **50**, 2315 (1928).
(14) J. C. L. Blagg and G. M. Murphy, *J. Chem. Phys.*, **4**, 631 (1936); K. H. Gelb and A. Lendle, *Z. Phys. Chem., Abt. B*, **32**, 463 (1936).
(15) A. Wheeler, B. Topley, and H. Eyring, *J. Chem. Phys.*, **4**, 178 (1936).
(16) S. W. Benson and R. Srinivasan, *J. Chem. Phys.*, **23**, 200 (1955).
(17) J. H. Sullivan, *J. Chem. Phys.*, **30**, 1291 (1959).
(18) N. N. Semenov, "Some Problems in Chemical Kinetics and Reactivity", Vol. 2, Princeton University Press, Princeton, N.J., 1959, pp 73 and 74.
(19) J. H. Sullivan, *J. Chem. Phys.*, **46**, 73 (1967).
(20) J. H. Sullivan, *J. Chem. Phys.*, **30**, 1577 (1959); **36**, 1925 (1962); **39**, 300 (1963).
(21) S. B. Jaffe and J. B. Anderson, *J. Chem. Phys.*, **49**, 2859 (1968); **51**, 1059 (1969).
(22) R. M. Noyes, *J. Chem. Phys.*, **48**, 323 (1968).
(23) R. Hoffmann, *J. Chem. Phys.*, **49**, 3739 (1968).
(24) L. C. Cusachs, M. Krieger, and C. W. McCurdy, *J. Chem. Phys.*, **49**, 3740 (1968).
(25) L. M. Raff, L. Stivers, R. N. Porter, D. L. Thompson, and L. B. Sims, *J. Chem. Phys.*, **52**, 3449 (1970).
(26) F. L. Minn and A. B. Hanratty, *J. Chem. Phys.*, **53**, 2543 (1970); *Theor. Chim. Acta*, **19**, 390 (1970).
(27) L. M. Raff, D. L. Thompson, L. B. Sims, and R. N. Porter, *J. Chem. Phys.*, **56**, 5998 (1972).
(28) J. C. Keck, *Adv. At. Mol. Phys.*, **13**, 85 (1967).
(29) S. W. Benson and T. Fueno, *J. Chem. Phys.*, **36**, 1597 (1962).
(30) R. N. Porter, D. L. Thompson, L. B. Sims, and L. M. Raff, *J. Am. Chem. Soc.*, **92**, 3208 (1970).
(31) J. B. Anderson and R. T. V. Kung, *J. Chem. Phys.*, **58**, 2477 (1973); **60**, 2202 (1974).
(32) H. S. Johnston, "Gas Phase Reaction Rate Theory", Ronald Press, New York, N.Y., 1966, Chapter 8.
(33) R. Marcelin, *Ann. Phys. (Paris)*, **3**, 120 (1915).
(34) E. Wigner, *J. Chem. Phys.*, **5**, 720 (1937).
(35) G. M. Murphy, *J. Chem. Phys.*, **4**, 344 (1936).
(36) J. Bigeleisen, *J. Chem. Phys.*, **18**, 481 (1950).
(37) V. Reich, Yale Computer Center Library, Memorandum No. 59, Yale University, New Haven, Conn., 1970.
(38) B. P. Stoicheff, *Can. J. Phys.*, **35**, 730 (1957), *Adv. Spectrosc.*, **1**, 91 (1959).
(39) G. Herzberg, "Spectra of Diatomic Molecules", 2nd ed, Van Nostrand, New York, N.Y., 1950.
(40) E. Wigner, *J. Chem. Phys.*, **7**, 646 (1939).
(41) D. L. Bunker, *J. Chem. Phys.*, **32**, 1001 (1960).
(42) J. B. Anderson, J. M. Henry, and R. L. Jaffe, *J. Chem. Phys.*, **60**, 3725 (1974).